Quaternary Science Reviews 249 (2020) 106593

Contents lists available at ScienceDirect

Quaternary Science Reviews

journal homepage: www.elsevier.com/locate/quascirev

Invited review

Climatic evolution in the Australian region over the last 94 ka - spanning human occupancy -, and unveiling the Last Glacial Maximum

P. De Deckker [a, *], M. Moros [b], K. Perner [b], T. Blanz [c], L. Wacker [d], R. Schneider [d], T.T. Barrows [e, f], T. O'Loingsigh [g], E. Jansen [h, i]

[a] Research School of Earth Sciences, The Australian National University, Canberra, ACT, 2601, Australia
[b] Leibniz Institute for Baltic Sea Research, Seestraße 15, 18119, Rostock, Germany
[c] Institute of Geosciences, Kiel University, Ludwig-Meyn-Straße 10, Kiel, 24118, Germany
[d] Laboratory of Ion Beam Physics (LIP), ETH, Otto-Stern-Weg 5, 8093, Zürich, Switzerland
[e] School of Earth, Atmospheric and Life Sciences, University of Wollongong, NSW, 2500, Australia
[f] School of the Environment, Geography and Geosciences, University of Portsmouth, UK
[g] School of Environment and Science, Griffith University, Nathan, QLD, 4111, Australia
[h] Department of Earth Science and Bjerknes Centre for Climate Research, University of Bergen, Jahnebakken 5, 5020, Bergen, Norway
[i] NORCE- Norwegian Research Centre/Climate and Bjerknes Centre for Climate Research, Jahnebakken 5, 5020, Bergen, Norway

ARTICLE INFO

Article history:
Received 28 January 2020
Received in revised form
9 September 2020
Accepted 10 September 2020
Available online xxx

Keywords:
Oceanic fronts
Leeuwin Current
Foraminifer faunal analysis
Marine isotopic stages
Last Glacial Maximum
Palaeoceanography
Sea-surface temperature
Moraines
Modern analogue technique
Subantarctic Front
G. ruber

ABSTRACT

The Quaternary is well known for being a period of the geological record that saw significant and alternating climatic fluctuations. Here, we concentrate on the last 94 millennia that saw Australia and its surrounding seas undergo significant environmental changes. Importantly also it is during that this period of time includes the arrival and settlement of humans in Australia.

Following on from Marine Isotopic Stage 4 (MIS4) that saw, over the period of 71-59 ka BP, a significant eustatic sea level drop (~100 m), low sea-surface temperatures as well as glacial conditions on land, Australia experienced wet conditions again, but eventually progressively entered into a glacial phase. By then, humans had arrived on this large continent and later the megafauna progressively became extinct. This paper describes in detail the climate over this period, based principally on the high-resolution record of two marine sediment cores located offshore of the southern Australian margin, and that are then compared with known events on land as well as other deep-sea cores. Particular emphasis is placed on the period that spans the Last Glacial Maximum (LGM), the extent of which thus far had been poorly defined in the Australian region. Emphasis is placed on the period from 34 to 14 ka to demonstrate that (1) the LGM, defined here as the period 24 to 18 ka, was not always extremely dry and cold, and (2) that people were able to live in inland Australia as water existed in places, despite generally cold conditions. We also show using a series of ten maps - at 2 ka intervals over the 34-14 ka period - the waxing and waning of oceanic fronts such as the Subtropical and Subantarctic Fronts, link sea-surface temperatures (SST) with periods of glacial expansion in the Australian Alps and Tasmania, as well as the South Island of New Zealand, and the extent of the Leeuwin Current down to south of Australia.

Aeolian dust was transported at sea over the main core site from ~26 to 18 ka period, pointing to arid conditions in Australia, but this period was punctuated by two significant reductions in dust transport to both core sites, coinciding with a retreat of the Subantarctic Front away from the Australian southern coastline, and slight SST shifts for a few centuries at ~24 and 22-21 ka BP. At the peak of the cold phase, from 23 to 18.4 ka, summer SST were of the order of 9 °C below that experienced during the middle of the Holocene at about 6 ka BP. A similar temperature drop was also experienced offshore the north-western corner of Western Australia. Periglacial activity dates for the Australian mainland and Tasmania pool around ~22 ka. On either side of the 24 ka event, the chain of lakes in the Willandra Lakes retained water and human activity was registered in the area. Elsewhere in Australia, water was present to sustain human populations during the cold and dry times. It is postulated here that northern Australia was at times quite wet, especially during MIS4.

* Corresponding author.
E-mail address: patrick.dedeckker@anu.edu.au (P. De Deckker).

https://doi.org/10.1016/j.quascirev.2020.106593

The cessation of the LGM is set on 18.4 ka from offshore southern Australia as confirmed for the deep-sea cores by several proxies, and more likely at 18 ka inland. Finally, we document that it took two millennia for "glacial" conditions to end in the Australian region as registered in our deep-sea core records, well after the lowest global sea level ~20.6 and 20 ka, respectively, started to rise.

There is also evidence of another very cold period determined on the Australian mainland, Tasmania and the South Island of New Zealand centred around 27 ka, after which time warmer conditions occurred before the start of the LGM. This is matched with our deep-sea records with very cold conditions and changes in oceanographic conditions.

Preamble

We wish to acknowledge the first inhabitants of Australia who have continuously lived on this continent for well over 50,000 years; that represents over 2500 generations! These people witnessed the ever changing climate, sea level changes and the passing of the megafauna, as well as vegetation and landscape shifts. We pay our respects to their knowledge and thank them for the privilege to unravel 'ancient' Australia which is now predominantly an arid continent, although in was quite different at times in prehistoric times.

1. Introduction

The last 100 millennia of Earth history has seen significant climatic changes, with progressive cooling to the Last Glacial Maximum (LGM), terminated by a rapid deglaciation transitioning into the Holocene. Prior to the low sea level (~100 m) seen at 64.8 ka BP (Grant et al., 2012), a significant drop of global temperatures and oceanic changes occurred. A more significant event during Marine Isotopic Stage 4 [MIS4; see De Deckker et al., 2019] also saw a substantial drop in temperatures and glaciation worldwide. A massive volcanic eruption occurred at Toba at 73 ka on the northern portion of Sumatra that saw volcanic ash, up to 1.5 m thick in places, being deposited as far west as India (Williams et al., 2009a,b), and this must have affected human population, especially in the Indonesian Archipelago. After that, climatic conditions improved, sea level rose, but eventually the Earth entered into a broad and long-lasting glacial phase.

By 55 ka BP, humans had already arrived in Australia (Clarkson et al., 2017, 2018; Veth, 2017; Wood, 2017) and settlement in the Willandra Lakes region of northwestern New South Wales (Fig. 1) was well established with evidence of human activity with *in situ* artefacts dated to ~49 ka BP and human burial just before 40 ka BP (Bowler et al., 2003, 2012). The chain of lakes at Willandra (Fig. 1) was full at times and thus provided ample food for humans (Bowler et al., 2012). Bowler et al. (2012) finalised years of investigations around the lakes area and provided much evidence, based on a robust chronology with numerous dates. A high lake level phase established by 60 ka BP (Bowler et al., 2003) and lasted until 47 ka BP (Bowler et al., 2012), after which time the lake dried out more frequently as the regional climate became drier (Barrows et al., 2020) (see discussion later). In contrast, in central Australia high lake levels at the extensive Kati Thanda-Lake Eyre (Phase III, occurred during much of MIS4 - see De Deckker et al. (2019), with a drainage basin of ~1.10×10^6 km^2 (Fig. 1), were progressively falling and by 53 ka BP the lake was dry (Magee et al., 2004). It was not until 43 ka BP that Kati Thanda-Lake Eyre (Fig. 1) started to fill again and this lake phase (Phase II), of lower importance compared to the previous one, lasted until ~36 ka BP. After that, a severe hydrological deficit occurred continent-wide that culminated during the LGM, and ended at the onset of the Holocene. Within the Lake Eyre Basin, Lake Frome's (Fig. 1) lake levels fluctuated (De Deckker et al., 2010; May et al., 2015; Cohen et al., 2015). Equally, Miller et al. (2016a,b) assessed point potential evapotranspiration for February plus March [PPET] from distinct regions of arid/semi-arid Australia, spanning mostly the last glacial/interglacial period based on the $\delta^{18}O$ composition of emu eggshells. The Holocene also saw some lake level fluctuations that led to much variation during the second half of the Holocene when Australia became under the influence of the El Niño Southern Oscillation [ENSO] (Donders et al., 2007; Moros et al., 2009; Perner et al., 2018).

The asynchrony of large lake levels across the Australian continent requires explanation. One consideration is that the Lake Eyre basin (Fig. 1) today receives most of its waters from the northern part of the continent in summer that are mostly generated by monsoonal activity (Magee and Miller, 1998), whereas moisture in the Willandra lakes region - for the periods discussed above – came from a mixture of directions, such as directly from the Southern Ocean (mostly during winter) as well as from the north when extensive cyclonic depressions travel as far as the southeastern part of Australia (Bowler, 1978a). This applies to the Darling River and its tributaries (such as the Lachlan River that feeds in the Willandra chain of lakes via Willandra Creek) (Fig. 1); this will be further discussed below.

Since large lakes deflate during dry phases and the surfaces undergo pedogenesis during dry events, there is a loss of sedimentary records and it has been necessary to rely on marine sedimentary records to provide a better and more complete picture of environmental changes both on land and at sea. The use of terrestrial proxies such as pollen, aeolian and fluvial clays recovered from marine cores can help decipher events on land and link with events that occurred at sea.

Elsewhere, in the much more arid portion of the Australian, continental-scale, dune fields were active at times, but are mostly inactive today and partly vegetated. The chronology of several dune fields is now fairly well known based on optical luminescence dates [OSL], a review of which is available in Fitzsimmons et al. (2013, and other references therein) and more recently in Hesse (2016). Finally, parts of highlands of Tasmania and a small area in the Snowy Mountains in southeastern Australia at times underwent glaciation and a broader area experienced periglacial processes, dated using cosmogenic isotopes (see Barrows et al., 2001, 2002; 2004; Macintosh et al., 2006).

Hence, Australia as a continent underwent significant changes over the last glacial/interglacial cycle in a variety of conditions covering the hydrosphere, the cryosphere, geomorphology and vegetation. Consequently, the first aim of our study is to provide information to better link marine and continental events in the Australian region, at least for the southern part of the continent and its adjacent ocean from where the largest proportion of studies have thus far concentrated. Two deep-sea cores located along the

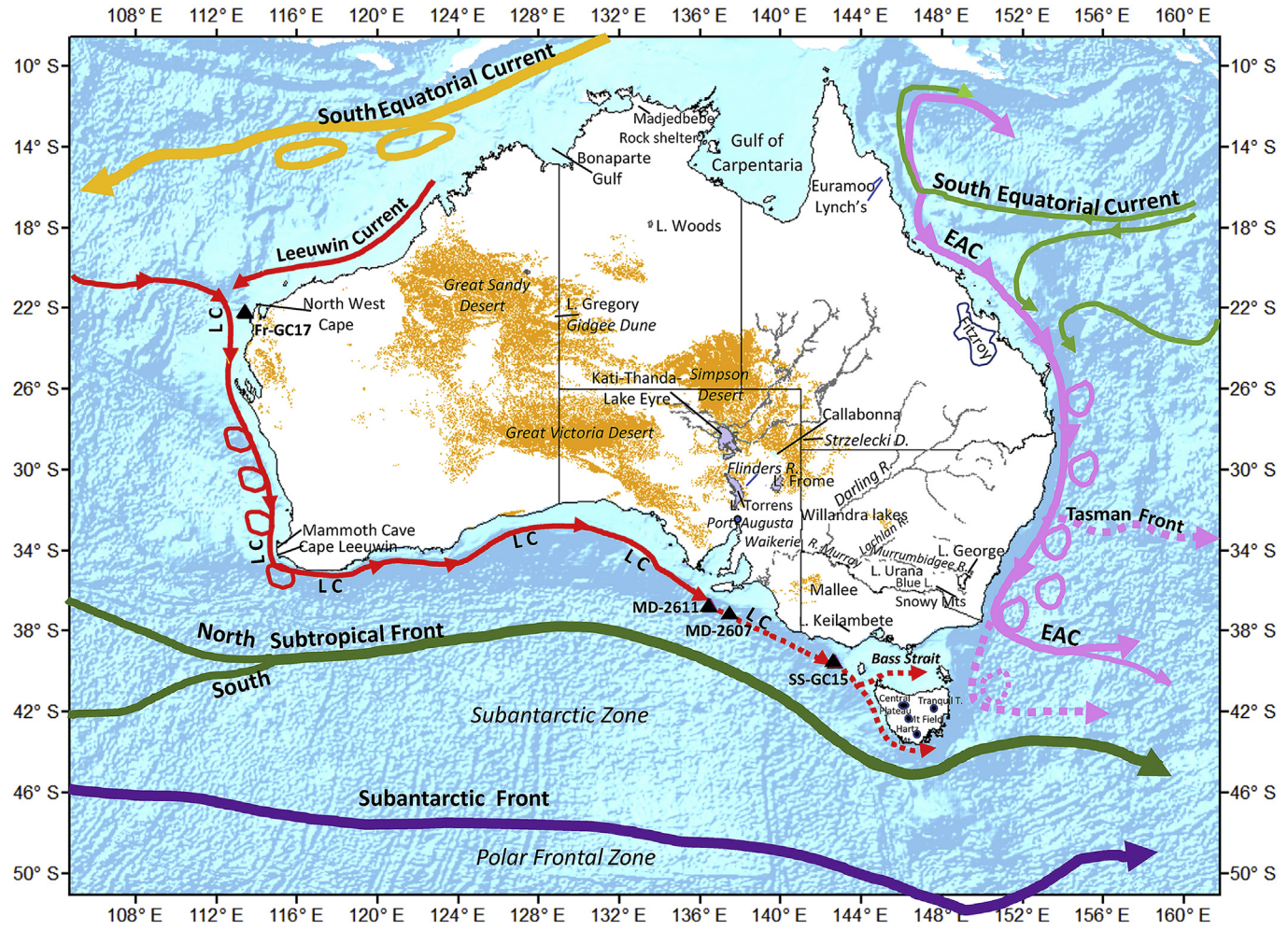

Fig. 1. Map of Australia and the surrounding oceans showing the position of the principal oceanic currents and fronts south of Australia, together with sites discussed in the paper. Note the eddies shown along the path of the 2 boundary currents Leeuwin Current (LC) and East Australia Current (EAC) are schematic as every year their positions change as they migrate poleward. The location of the 4 deep-sea cores discussed in the paper are also shown.

southern margin of Australia were selected for this study and were sampled at high resolution for a large variety of climatic and palaeoceanographic proxies.

2. Oceanographic setting

The ocean adjacent to the southern coast of Australia is commonly called the Southeast Indian Ocean. Further south, the ocean is called the Southern Ocean that circumnavigates Antarctica. The southern coast of Australia is bordered by the southeast Indian Ocean and the Southern Ocean. Middleton and Bye (2007) provide a good synthesis of the currents and water masses offshore Kangaroo Island and adjacent coastlines extending as far as Victoria. It is in these two areas that our deep-sea cores were taken (Fig. 1). More information on the currents and oceanic fronts discussed in this paper is available in the supplementary section.

3. Material and methods

3.1. Marine cores

Marine sediment core MD03-2611 (herein called 2611) (36°43.8′S, 136°32.9′E) was obtained during the AUSCAN cruise with *RV Marion Dufresne* in 2003 from a small plateau south of Kangaroo Island at 2420 m water depth (Fig. 1). This core is located opposite the mouth of the River Murray which is joined by the Darling River to drain a ~1.1 × 10^6 km^2 basin (Fig. 1), called the Murray Darling Basin. The core lies below the path of the Leeuwin Current (LC).

Further down the path of the LC - when prominent -, about 600 km eastwards and at a slightly higher latitude from site MD03-2611, is the site for core SS0206-GC15 (38°11.26′S, 142°24.62′E, almost due south of the town of Warrnambool; Fig. 1). It was obtained in 2006 at a 907 m water depth with the *RV Southern Surveyor* (Fig. 1).

The 11.67 m long core 2611 is described in Hill and De Deckker (2004) who also provide information on the core site. It is located to the NW of many of the ancient courses of the palaeo-River Murray (see Hill et al., 2009) that would have supplied terrigenous material to the core site as a result of lateral transport (see Middleton and Bye, 2007; Bayon et al., 2017). Samples taken at close intervals from the 'working half' of the core were processed for planktic foraminifera faunal analyses, stable isotopes on two foraminifera species (*Globigerina bulloides* and *Globigerinoides ruber*), radiocarbon dating on selected planktic foraminifera, XRD analyses of selected levels and for the extraction of alkenones. A U-channel was taken from the middle of the 'archive half' of the core for XRF scanning.

Core SS02/06-GC15 (herein called GC15) consists of uniform, dark grey clay and is 5.55 m long. A U-channel was taken in the middle of the 'work half' of the core and was also processed at the Leibniz Institute for Baltic Sea Research in Warnemünde for XRF core scanning analysis using the same core scanner facility listed above, and afterwards, the U-channel was sampled at close intervals for extraction of planktic foraminifera and examination their faunal composition, and radiocarbon dating of planktic foraminifera. Additional samples were processed for alkenone extraction at close intervals and analysed at Kiel University.

We will also be referring extensively to core Fr10/95-GC17 that is located offshore the northwestern tip of Western Australia (Fig. 1) as a number of proxies were already obtained for that core (van der Kaars and De Deckker, 2002, 2003; De Deckker et al., 2014) and which are worthy of comparison with the two cores mentioned above.

3.2. Elemental ratios obtained from high-resolution XRF scanning of the cores

The U-channels for both cores were processed at the Leibniz Institute for Baltic Sea Research in Warnemünde for XRF core scanning analysis using an ITRAX core scanner (Cox Analytical Instruments, Sweden). A detailed description of the ITRAX core scanner is given in Croudace et al. (2006). U-channels were taken from core liners and scanned at 0.5 cm resolution, using a Cr-tube (60 kV, 30 mA) and 15 s counting time. The X-ray fluorescence (XRF) scanner collects element profiles along the entire length of the core and relevant results for titanium are presented as well as counts per second (cps). More information on the equipment used is presented in the supplementary section. We concentrated on titanium (Ti) in an attempt to identify the presence of airborne dust in the core as established already by a number of studies (Weltje and Tjallingii (2008); Stuut et al. (2014), the latter for sediments in a core taken offshore Western Australia; core MD00-2361, located adjacent to core site Fr10/95-GC17, (Fig. 1). Additional information is available in the supplementary section as well as in Stuut et al. (2019).

3.3. X-ray mineralogy of bulk sediment samples

X-ray diffraction was used on a large number of samples from core 2611 (see also data repository files) to determine the percentage of terrigenous (airborne) quartz in samples from the core and is further discussed in the Supplementary Section.

The quartz content was determined using X-ray diffraction (XRD) analysis following the procedures described in Moros et al. (2004) and De Deckker et al. (2012, supplement sections). A PHILLIPS PW1830 diffractometer (Co Ka-radiation), coupled to an automatic sample changer was used. Initial bulk samples were scanned from 0 to 80°Θ but, for the purpose of this study, a spectrum from 20 to 40° 2Θ which involves the major peaks of quartz was used. The raw data were evaluated using the MacDiff4 program (for details refer to http://servermac.geologie.uni-frankfurt.de/Neu/Staff/Homepages/Petschick/Rainer.html).

3.4. Radiocarbon chronology

The chronology for samples taken from both cores is based on accelerator mass spectrometry (AMS) radiocarbon (^{14}C) dates. We used a mixture of planktic foraminifera of *Globigerinoides ruber* and *Globigerina bulloides* that were analysed at the Poznan Radiocarbon Laboratory (Poland; samples with Poz prefix) as well as at the Swiss Federal Institute of Technology Zurich (prefix ETH), the Australian Nuclear Science and Technology Organization (OZH prefix) and the Australian National University (S-ANU prefix) Radiocarbon Laboratories. In total, 78 samples were analysed from core 2611 and 38 from core GC15 (Supplementary Tables 3 and 4). Overall, the planktic foraminifer record is resolved on average at 40 years (MD03-2611) and 80 years (SS0206-GC15) per sample, the difference being due to the different rates of sedimentation in both cores and the intervals sampled. For more information, refer to the supplementary sections 5 and supplementary Tables 3 and 4

AMS ^{14}C dates were calibrated using the Marine13 calibration curve (Reimer et al., 2013) in CALIB 7.0.2 software (Stuiver and Reimer, 1993) applying local reservoir age corrections using two approaches: 1) Delta R of 40 years throughout the Holocene back to 14 ^{14}C ka BP and 2) Delta R of 200 years and 300 years for the time intervals 14 to 18 ^{14}C ka BP and older than 18 ^{14}C ka BP, respectively, when taking into account the larger reservoir age observed by Sikes and Guilderson (2016) (see further discussion in supplementary section 2).

3.5. Isotopic analysis of planktic foraminifera

Two planktic species were selected from core 2611 from the dry residues used for faunal analysis: *Globigerinoides ruber* (white) and *Globigerina bulloides*. These species were analysed separately for their stable isotopic composition. About 6–10 specimens of the fraction >150 μm were crushed and cleaned in an ultrasonic bath. All isotope analyses were carried out at the GMS Laboratory of the Bjerknes Centre for Climate Research at the University of Bergen, using a Finnigan MAT 251 mass spectrometer equipped with an automatic 'Kiel device' preparation line. The reproducibility of isotope measurements is ±0.07‰, based on replicate measurements of carbonate standards. All results are reported δ^{18}O in ‰ vs. VPDB using NBS19 as a standard.

Using the δ^{18}O for both species from the same level in each core provides information on surface ventilation and water column stratification changes ($\Delta\delta^{18}$O (*G. ruber-G.bulloides*, with values *G. bulloides* subtracted from those of *G. ruber*) of as already discussed in Perner et al. (2018).

3.6. Faunal assemblages of planktic foraminifera

For faunal assemblages of planktic foraminifera assemblage analysis, we used about 5 g of dry sediment from both cores that was wet sieved through a 150 μm sieve. On average, 400 planktic foraminifera were counted from the dry residue of the >150 μm fraction and identification down to species level, using a stereomicroscope, followed the taxonomy of Parker (1962). We identified a total 19 planktic foraminiferal species (Supplementary Table 1).

Several foraminifera assemblages are characteristic of specific water masses, as well as associations with oceanic fronts/boundaries. These relate to (1) the Leeuwin Current and associated tropical water indicators, (2) the Subtropical Frontal Zone; (3) the Antarctic Intermediate water, and (4) subpolar waters in association with the Subtantarctic Front. More information on those foraminifera taxa indicators are presented in Supplementary section 2 and are already partly discussed in Perner et al. (2018).

Closer to Tasmania, King and Howard (2003) examined the planktonic foraminifer assemblages recovered from core tops as well as 3 sediment traps along a N-S transect that crosses several oceanic boundaries. A summary of the salient features recognized by many of the foraminifers is presented in Supplementary Table 2 and Supplementary Figure 1. Those findings are used here to estimate the approximate position of the STF and SAF with respect to the core sites.

3.7. Sea-surface temperature reconstructions

3.7.1. Sea-surface temperature estimated by alkenometry

Reconstruction of sea-surface temperatures (SST) based on alkenone analyses was carried out at the Biomarker Laboratory at the Institute of Geosciences, Kiel University, at sample intervals of 2 cm for core 2611 and 1 cm for core GC15. Long-chained alkenones (C37) were extracted from homogenised, 2–3 g of bulk sediment, using an Accelerated Solvent Extractor (Dionex ASE-200) with a mixture of 9:1 (v/v) of dichloromethane:methanol (DCM:MeOH) at 100 °C and 100 bar N2 (g) pressure for 20 min. Extracts were cooled to about −20 °C and subsequently taken to near dryness by vacuum rotary evaporation at 20 °C and 65 mbar. We used a multi-dimensional, double gas column chromatography (MD-GC) set up with two Agilent 6890 gas chromatographs for identification and quantification of C37:2 and C37:3 ketones (Etourneau et al., 2010). Quantification of the individual compounds was achieved with the addition of an internal standard prior to extraction (cholestane [C37H48] and hexatriacontane [C36H74]). The relative proportions were obtained using the peak areas of the two different compounds. The UK'_{37} index was calculated using the equation (Prahl and Wakeham, 1987): $UK'_{37} = (C37:2)/(C37:2+C37:3)$, which was subsequently translated into SST (error bar 1 °C) following a global calibration (Müller et al., 1998): $SST\ (°C) = (UK'_{37}-0.044)/0.033$.

However, it is noteworthy that Sikes et al. (2005), who analysed the occurrence of alkenone biomarkers over the 1996–1997 period (covering late winter to autumn) in 2 sediment traps located in subtropical and subantarctic waters south of New Zealand, showed that a complex set of parameters such as nutrient and light levels can cause the temperature signal derived from the ketone unsaturation index in to deviate from known calibrations. Discussion will be provided later into the possibility of the alkenone-derived SST signal to represent a summer temperature.

3.7.2. Sea-surface temperature estimated from planktic foraminifera assemblages

Sea-surface temperatures (SST) were estimated from the planktic foraminifera assemblage data using the modern analogue technique (MAT), in conjunction with the AUSMAT-F4 database established by Barrows and Juggins (2005). Estimates were made for mean annual temperature (T_{mean}), the coldest month (T_{min}) and the warmest month (T_{max}). Each SST estimate was calculated as the mean of the 10 best analogues from the global database, using the square chord distance as the dissimilarity coefficient, with squared chord distances of <0.2 indicating good modern analogues

4. Previous work

Information on previous work carried out in the region offshore southern Australia of relevance to the study of the deep-sea cores discussed below is presented in the supplementary section.

5. Results

5.1. Chronology

The chronology for the Holocene part of core 2611 is published in Moros et al. (2009) and updated in Perner et al. (2018). The age-depth relationship for the interval 33 to 10 ka is presented in De Deckker et al. (2012). In order to improve the chronology for the last deglaciation, additional AMS ^{14}C dates were obtained for the time interval 25 to 7 ka (Moros et al., submitted). Additional dates were also obtained on older parts of the core and are presented in Supplementary Table 3.

Sikes and Guilderson (2016), assessed marine reservoir ages (MAR) for cores located north and east of New Zealand in the southwestern Pacific Ocean by comparing with tephra ages on land (with radiocarbon dates for organic deposits associated with those layers) also found in marine cores. Their findings relate to six distinct periods of tephra deposition with calibrated years of ~25.6 ka, ~17. 9 ka, ~14.0 ka, ~9.3 ka, ~8.0 ka and ~5.5 ka. Based on their study, Sikes and Guilderson (2016) concluded that the glacial reservoir for subtropical waters was ~700 years older than the atmosphere at ~25 ka BP and, for the early deglaciation (~18-14 ka BP), reservoir age was ~600–700 years, and for the Holocene it was similar to today's range. These findings for the western Pacific Ocean appear lower than the modelled reservoir ages in Butzin et al. (2020; Fig. 3; refer to Supplementary Figure 1 for visual comparison and the supplementary information). Since there is so little information on the LGM reservoir age for the Australian region, apart from the work of Sikes and Guilderson (2016) for the western Pacific, we are adding an additional 260 years to the original reservoir ages of 440 years (see Supplementary Table 3) for samples from ~18 cal ka BP to 25 ka, and then 160 years for the period spaning 18 to 14 cal ka BP, and with no addition for younger samples. We note that the range of (1 σ) errors obtained during calibration overall is lower than the values to be added.

Nevertheless, we are aware that using a reservoir age of 700 years for all levels deposited before 25 ka BP may one day need to be re-examined. For example, when % the abundance of *G. bulloides* is high, when the front is close to the core site and perhaps indicating upwelling, reservoir ages may be > 700 years. In the opposite situation, when the abundance of *G. ruber* and *G. rubescens* are high in the core, thus indicating the presence of water originating from the tropics via the LC, reservoir ages may be < 700 years. In addition, different levels of water column stratification, as well as changes in oceanic front influences such as for the SAF (as indicated by the subpolar foraminifera faunal assemblages) and the STF (as indicated by *N. incompta* %) potentially affect reservoir ages over the core site.

There are marked sedimentation rate changes from c. 800 cm downcore in 2611 which extends beyond the radiocarbon limit (c. 51 ka; Supplementary Figure 2). The most salient feature is that higher rates are registered for the two periods of low sea level that coincided with glacial/cold conditions (MIS 2 and 4). For the time interval from c. 58 ka (from c. 950 cm downcore), covering MIS4, the chronology of the nearby core MD03-2607 (De Deckker et al., 2019) was projected onto 2611 based on correlation of marked changes in alkenone-derived SSTs, planktic foraminifera and oxygen isotope data of *G. bulloides* (Fig. 2; Supplementary Figure 3, Core GC15 covers the last 25 ka, the chronology of which for the last 7.6 ka is already published in Perner et al. (2018) and for 25 to 7.6 ka in Moros et al. (submitted to *Quaternary Research*), respectively. All the dates for that core are presented in Supplementary Table 3 with reservoir ages as for core 2611.

Concerning core Fr10/95-GC17 taken offshore Northwest Cape in NW Western Australia, we are not changing the already-published chronology (De Deckker et al., 2014) as it is based not only on AMS ^{14}C dates obtained from planktic foraminifera but was combined with some Optically-Stimulated Luminescence (OSL) dates (see Olley et al., 2004) that were obtained originally to counteract the MRAs.

5.2. Sedimentation rate

Supplementary Figure 2 shows the sedimentation rates for core 2611 over the last 94 ka and the salient feature is that during the 'glacial phases' sediment deposition at the core site was higher when sea level was low (~134 m at the maximum of MIS2 and

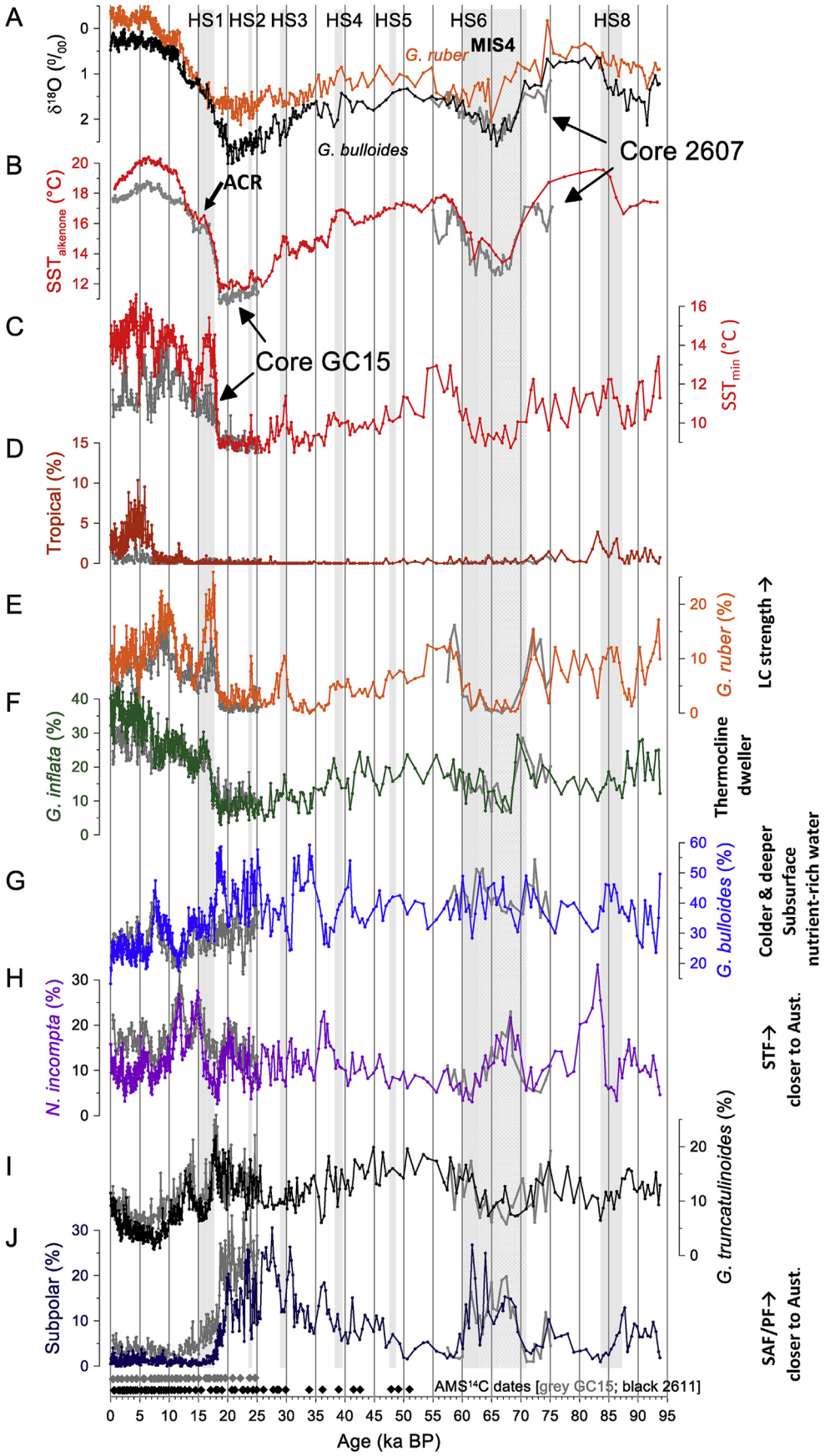
A
B
C
D
E
F
G
H
I
J
HS1 HS2 HS3 HS4 HS5 HS6 HS8
MIS4
G. ruber
G. bulloides
Core 2607
ACR
Core GC15
δ18O (‰)
SSTalkenone (°C)
SSTmin (°C)
Tropical (%)
G. ruber (%)
G. inflata (%)
G. bulloides (%)
N. incompta (%)
G. truncatulinoides (%)
Subpolar (%)
LC strength →
Thermocline dweller
Colder & deeper Subsurface nutrient-rich water
STF→ closer to Aust.
SAF/PF→ closer to Aust.
AMS14C dates [grey GC15; black 2611]
Age (ka BP)

~100 m during MIS4 (see De Deckker et al., 2019). The rate is higher during MIS2 compared to MIS4 probably because the mouth of the River Murray was closer to the core site (refer to Hill et al. (2009; Figs. 2 and 3) for reconstructed migrations of palaeo-meanders of the Murray on the Lacepede Shelf).

5.3. Oxygen isotope data

The $\delta^{18}O$ of both *G. ruber* and *G. bulloides* for core 2611 are compared in Fig. 2A. During the Holocene, there is an almost 1 per mil difference ($\Delta\delta^{18}O$) between the 2 data sets, suggesting stratification of the water column. In contrast, for the period of 18 to 15 ka, $\delta^{18}O$ values are almost identical, pointing to an absence of stratification, perhaps implying wind-driven water mixing of the upper few hundred meters. Before this, the water column was strongly stratified, with the most amplified period being between 25 and 20 ka. There are also two periods of reduced stratification around 43-42 ka and just before 51 ka.

5.4. Alkenone SST

Comparison of the sea-surface temperature record obtained from the Müller et al. (1998) mean annual calibration with the modern analogue temperatures shows more of a correspondence with summer temperature (Supplementary Figure 7). although we must concede that there is a widely accepted concensus that $U^{K'}_{37}$ signal represents a mean annual temperature (Müller and Fisher, 2001; Pelejero et al., 2006; Calvo et al., 2007; the latter two studies being for the Australian region). However, the study of Sikes et al. (2005) on sediment traps monnitored offshore eastern New Zealand indicate highest levels of alkenone flux during Spring and Summer. However, despite this seasonal variability, $U^{K'}_{37}$ strongly reflects mean annual SST (Sikes et al., 2005). Hence, we interpret that the SSTs obtained from alkenometry from our cores to represent a mean annual signal (see more information below).

Two features emerge in the SST estimates from core 2611 presented in Fig. 2B. The last 12 ka have been the warmest during the last 94 ka. Temperature rapidly rose after the Antarctic Cold Reversal (ACR; from 14.7 to 13 ka ago) to eventually reach a peak at ~6 ka. After this time, there is a progressive temperature drop also seen in the adjacent core 2607 (Calvo et al., 2007). The second salient feature is that from ~57 ka, SST progressively fell, with some fluctuations, down to 18.6 ka BP. There are at least six periods which saw a SST increase and these are similar in time with Heinrich Stadials (HS) 8, 6 to 2 recognized in the northern hemisphere (Broecker, 2002). Note for clarification that Heinrich events that refer to armadas of iceberg discharges in the North Atlantic Ocean (Heinrich, 1988) are not seen in the Southern Hemisphere. The broadest and largest SST rise (~5 °C) occurred during HS1, starting at 18.6 ka and lasted until 16 ka, then fell by the time of the ACR.

Finally, it is noteworthy that the high SST (~19.5 °C) at ~57 ka was not matched until 10 ka BP. Although the SST data for core GC15 only spans the last 25 ka, it shows the same trend as for core 2611, but in general SST was of the order of 1 °C lower. This is understandable since that core is located further south in the southeast Indian Ocean (see Fig. 26 in Wijffels et al., 2018). The interesting feature is that during the temperature rise straight after 18 ka BP, values were almost identical for 5 millennia, except during the ACR when they diverged once more by ~1 °C.

5.5. Planktonic foraminifera SST

The temperature of the warmest month (T_{max}) and the coldest month (T_{min}) have similar profiles and the coldest month has a slightly lower amplitude (~1 °C) (Fig. 2; Supplementary Figure 7). SST gradually declines from ~55 ka to the LGM where SST is colder than the core top by ~5–7 °C. There is a distinct Holocene maximum 1.5–2 °C warmer than present with subsequent progressive cooling. The SST estimates of core 2611 differ from the alkenometry in several aspects. SST is not as high as seen in MIS5a in the $U^{K'}_{37}$ estimates. The Holocene record of core GC15 shows a greater difference with the $U^{K'}_{37}$ and is cooler by about 2 °C (Fig. 2C), but also is about 1 °C lower than the $U^{K'}_{37}$ SST during the deglaciation.

5.6. The record of the Leeuwin Current

The record of the Leeuwin Current (LC) reaching the core site (Fig. 2E) is somewhat ambiguous when examining the percentage of the tropical faunas reaching the site of core 2611. After 7 ka BP, percentages start to increase and then peak just after 5 ka BP with values progressively falling afterwards. Additional information is provided in more detail in Perner et al. (2018). Concerning core GC15, tropical faunas were rarely encountered (see Fig. 2D) and this is understandable as the LC would have had to extend significantly to reach the south coast of Victoria (see Fig. 26 in Wijffels et al., 2018 and Supplementary Figures 4-6). In core 2611, during the SST high near the beginning of the record, tropical faunas were present but in low (<5) percentages.

Another and more sensitive LC indicator is *G. ruber* in both cores, simply because this species can live in cooler waters than the tropical species. The abundance of *G. ruber* (Fig. 2E) suggests that waters from the Indonesian Throughflow (ITF) extended along the southern margin of Australia via the LC. This current was the strongest during the equivalent of HS1 with values reaching 20% or more, but it consistently reached core site 2611 during the equivalent of the Heinrich Stadials (HS8-1). *G. ruber* were rare between the equivalent of HS2 and HS1 before HS5 when SST (both summer and winter) were very low (Fig. 2B and C). The highest *G. ruber* percentage recorded over the 94 ka period occurred straight after 18.4 ka BP, and lasted 2 ka before falling below 10%. This was the response (or the link) to a global trigger that led to the abrupt termination of the glaciation to be discussed later.

5.7. Behaviour of the STF indicator N. incompta

N. incompta, also referred to as *N. pachyderma* (dextral coiling version), is reported as a subpolar to transitional species (Bé, 1977; Bé and Tolderlund, 1971) which preferentially dwells just below the thermocline (Fairbanks et al., 1982). This species is also found

Fig. 2. Various proxy records from cores MD03-2611 and SS0206-GC15. Note that the latter core site is positioned further south and, at times, both sites occur below the path of the Leeuwin Current (LC). The grey lines relate to core GC15, whereas the core 2611 records are in different colours relate to core 2611. The records span the 0 to 94 ka period and is controlled by ample AMS radiocarbon dates (79 dates shown in black for core 2611 and 34 dates shown in grey for core GC15) with positions in both cores displayed at the bottom of figure. A. $\delta^{18}O$ record of two planktic foraminifera species (orange for *G. ruber* and black for *G. bulloides*) from core 2611; in grey is a plot of the *G. bulloides* record from core MD03-2607 from De Deckker et al. (2019) that was used to correlate both cores; **B.** mean annual alkenometry SST record in °C (note the record of GC15 shown in grey only spans the last 25 ka); **C.** T_{min} SST record in °C using the AUSMAT-F4 database; **D-J:** relative percentages of various foraminifera species recovered from both cores: **D.** tropical species assemblages; **E.** relative percentages of *G. ruber* that is indicative of the presence of the Leeuwin Current above each core site; **E.** *G. inflata*; **G.** *G. bulloides;* **H.** *N. incompta;* **I.** *G. truncatulinoides;* **H.** subpolar species assemblage. The broad, vertical grey bars represent the extent in time of Heinrich Stadials (HS) 1–8). The broad, vertical grey bars represent the time periods of the Northern Hemisphere Heinrich stadials 1–8, and the darker grey broad band represents the extent of MIS4 (De Deckker et al., 2019). The Antarctic Cold Reversal (ACR) is also indicated.

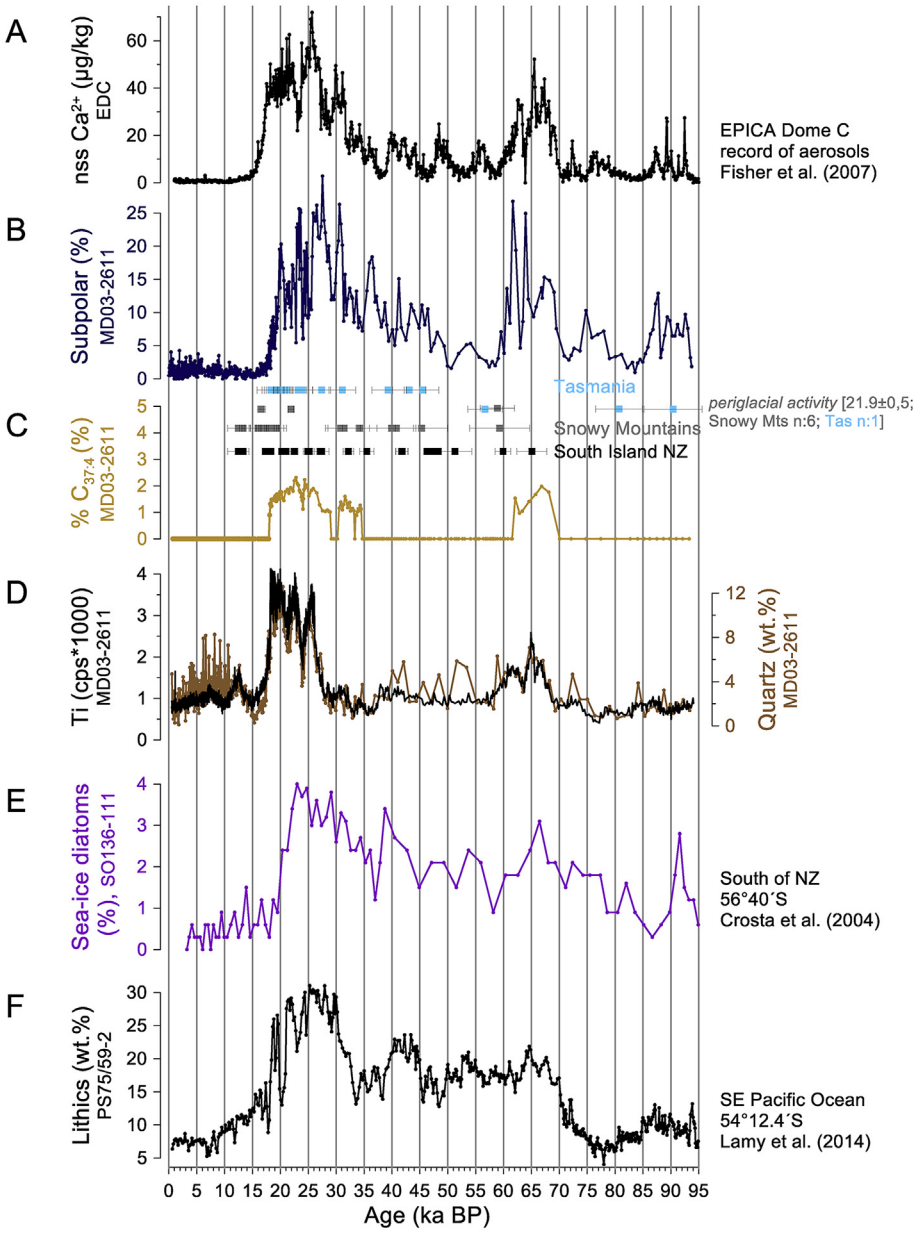

Fig. 3. Comparison of selected proxies from core MD03-2611 and related records for the period encompassing the 0 to 94 ka period. **A:** the non-sea salt component of calcium [nssCa = Ca-(Ca/Na)sea water *Na] in the EPICA Dome C core (EDC) (De Angelis et al., 2012); **B:** the percentage of subpolar foraminifera indicators in core 2611; **C:** exposure ages and errors for moraines in Tasmania (upper panel in blue), for the Snowy Mountains (3rd panel in grey), the South Island of New Zealand (lower panel in black), and exposure ages for block deposits in Australia (2nd panel); **D:** the percentage of $C_{37:4}$ compounds in core 2611; **E**: the presence of Ti (shown in black) recorded in counts per seconds ×1000 from core 2611, and the weight per cent of quartz (shown in brown) in core 2611; **F:** the percentage of sea-ice diatoms in core SO1-111 (56° 40′S, 160°14′ E; Crosta et al., 2004); **G:** the weight per cent of lithics recovered from core PS75/59-2 (54°12.90′S, 125°25.53′W; Lamy et al., 2014).

inhabiting subantarctic waters with surface water temperatures ranging between 10° and 18 °C. Two peaks of *N. incompta* occur at 15 ka and another at ~12 ka, when the percentage of *G. ruber* was low (Fig. 2E, Supplementary Figure 4) and T_{min} fell in parallel (Fig. 2C). During those periods, the STF had migrated north but not to the same extent as indicated by the percentages of subpolar species (Fig. 2J) and *G. bulloides* (Fig. 2G), prior to those times (refer also to Supp. Figs. 4-6). Equally, during MIS4, the percentages of *N. incompta* are high, especially at the beginning of that interval.

5.8. Faunal changes of planktic foraminifera

The high-resolution analysis of the planktic foraminifers encountered in both southern cores provides useful and detailed information on the export of heat from the tropics, viz. the Indo-Pacific Warm Pool. In addition, the tropical and subpolar species assemblages again are useful informers of the arrival of tropical water - via the LC - above the core sites and also the presence of the SAF, respectively near the core sites (Supplementary Figures 4-6 and Table 2). Some of the relevant palaeoecological and palaeogeographical implications are provided in the discussions that follow and were used in the preparation of the palaeogeographic maps (Fig. 7A–J) presented herewith.

Examination of Figs. 2J and 3B shows that the percentages of subpolar species are generally high (>10%) from about 70 ka until 61 ka, increasing from 47 ka to reach maximum at ~27 ka, but

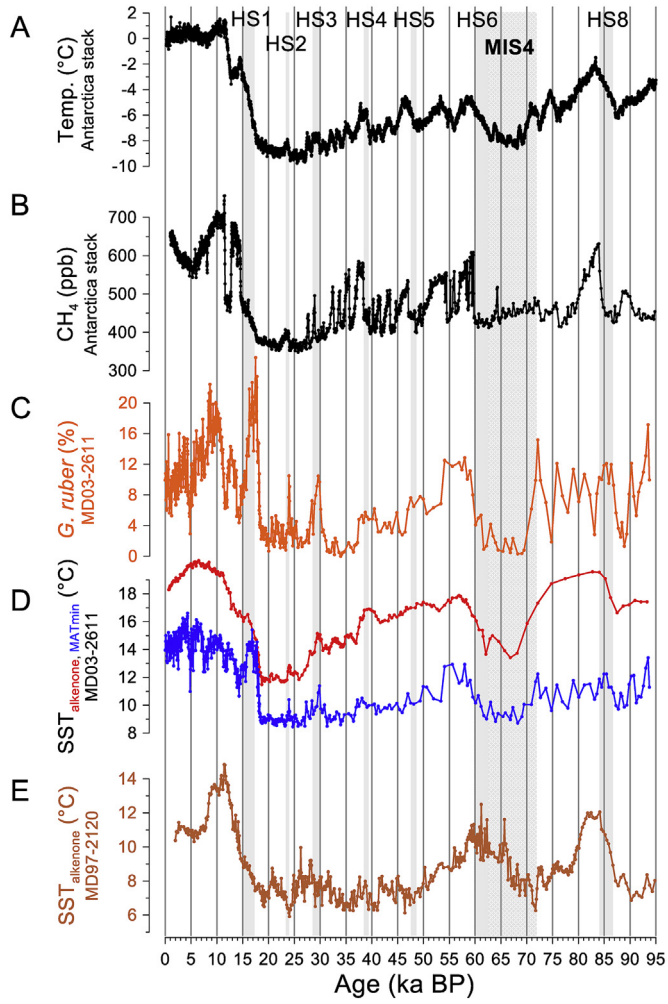

Fig. 4. Comparison of selected proxies for the period encompassing the 0 to 94 ka period. **A**: temperature stack for 5 Antarctic ice cores complied by Parrenin et al. (2013); **B**: smoothed record of CH_4 from Antarctic ice cores complied by Köhler et al. (2017); **C**: relative percentages of the foraminifera *G. ruber* that is indicative of the presence of the Leeuwin Current above core site 2611; **D**: alkenone SST record in °C from core 2611; **E**: T_{min} SST record from core 2611; **G**: alkenone SST record from core MD97-2120 (Pahnke et al. (2003)). The broad, vertical grey bars represent the time periods of the Northern Hemisphere Heinrich stadials 1–8, and the darker grey broad band represents MIS4 (De Deckker et al., 2019).

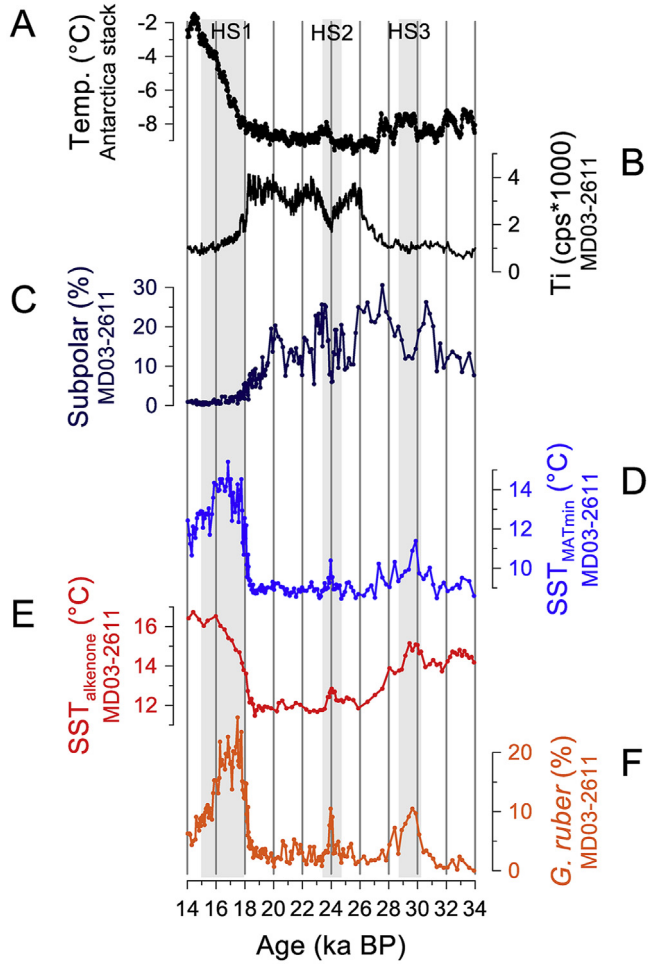

Fig. 5. Comparison of selected proxies from core MD03-2611 against selected records for the period encompassing the 14 to 34 ka period. **A:** Temperature stack record for 5 Antarctic ice record from Parrenin et al. (2013); **B:** the presence of Ti (shown in black) recorded in counts per seconds ×1000 from core 2611 obtained by XRF scanning of core 2611; **C:** percentages of the subpolar species foraminifer assemblage in core 2611; **D:** T_{min} SST record from 2611; **E**: alkenone SST record from core 2611; **F**: relative percentages of the foraminifera *G. ruber*. The broad, vertical grey bars represent the time periods of the Northern Hemisphere Heinrich stadials 1–8.

remaining high until 18.6 ka, after which time values are close to zero in core 2611 and slightly higher in core GC15 (Figs. 2 and 5). The highest percentages of subpolar species occurred between 28 and 26 ka (>20%) and fluctuate after this. The SAF did wax and wane near the Australian continental margin after that period until 18.6 ka. Note the coincidence of SST fluctuations with the waxing and waning of the SAF.

5.9. Change of water quality at core site 2611

The pronounced increases in % of C_{37-4} during MIS4 and from 35 to 20 ka BP (Fig. 3D) could be either due to very cold subpolar waters above the core site or due to the arrival of lower salinity waters coming into that area (or both) when the Subantarctic Front was at its northernmost position. The other possibility is that the C_{37-4} signal relates to the supply of Murray River water to the core site during periods of low sea level. Few C_{37-4} records exist for the Southern Ocean making it difficult to interpret whether this is an oceanographic-related feature (Ho et al. (2012); Jaeschke et al. (2017)).

5.10. Non carbonate record (core 2611)

Two proxies were used to determine the supply of aeolian dust to the site of core 2611: (1) the continuous measurements of titanium (Ti) in the core obtained by XRF-core scanning (Fig. 3E, black curve, Supplementary Figure 9); and (2) the percentage of quartz obtained from 390 samples using XRD mineralogical measurements of the same core (Fig. 3E, brown curve). Titanium is considered to be indicative of a supply of aeolian material deposited at sea as it is a conservative element that is restricted to lithogenic sediments and inert to diagenetic process (see Tjallingii et al., 2007; Stuut et al., 2014). Large quartz grains can only have been deposited at sea via aeolian transport because the core site is located too far away from the Australian coast, even during the period of low sea level. For additional information, refer to De Deckker et al. (2012).

Both proxies for aeolian activity show a similar signal for the period of 27 to 18.4 ka in core 2611, suggesting deflation and

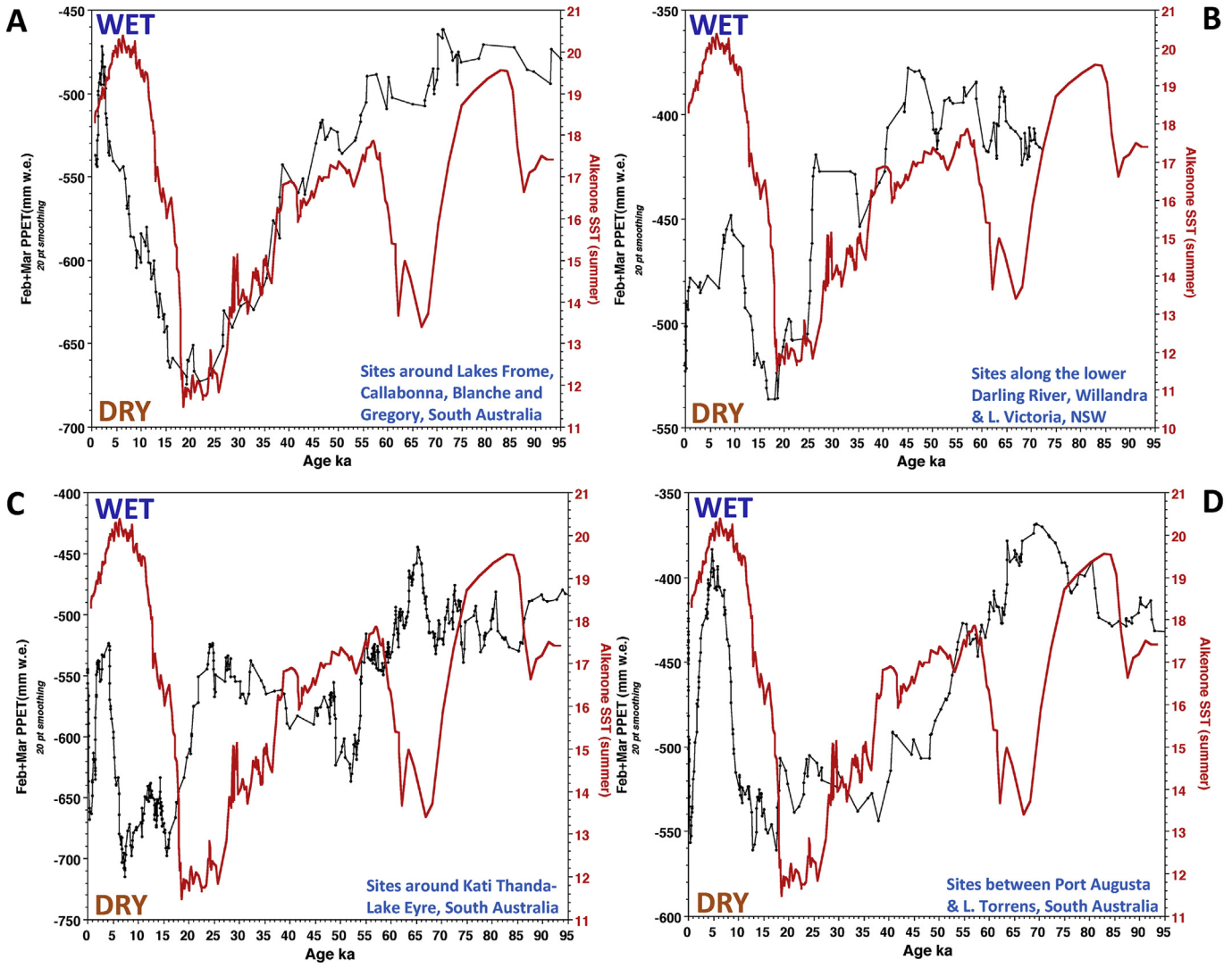

Fig. 6. Plot of alkenone SST in core MD03-2611 based on alkenometry for the last 95 ka against the reconstruction of the assessed point potential evapotranspiration for February plus March [PPET] for distinct regions of arid/semi-arid Australia (Miller et al., 2016) using a 20 point running mean; **(A)** sites around Lakes Frome, Callabonna, Blanche and Gregory in central South Australia; **(B)** sites along the lower Darling River, Willandra and Lake Victoria, NSW; **(C)** sites around Kati Thanda-Lake Eyre, South Australia; and **(D)** sites between Port Augusta and Lake Torrens, South Australia. Note the record in B does not extend as far back as 94 ka.

therefore arid conditions in inland Australia. The Ti counts and the quartz percentages are very pronounced for this period (Fig. 3D, Supplementary Figure 9), but it was punctuated by two significant reductions in lithic/clastic sediment, coinciding with slight temperature increases at the sea-surface at 24 and 22-21 ka BP (Fig. 2B and C). The three main peaks increase in height from 25 to 27 to 23 to 17–20 ka BP. There is also indication of deposition of dust to the core site during MIS4, with a peak at 65 ka. This coincides with the peak of the glaciation in the South Island of New Zealand (Schaefer et al., 2015). Dust deposition declined during the deglaciation and into the Holocene. This will be discussed later.

6. Interpretation of the various proxies and comparison with other (mostly high-resolution) records in the southern hemisphere

6.1. The ice core records from Antarctica

The reconstruction of millennial changes in dust emission, transport and regional sea ice coverage using the EPICA ice cores provided by Fisher and 28 other authors. (2007) shows a similar pattern (Fig. 3A) to the subpolar foraminifera species abundance from core 2611 (Fig. 3B), reflecting colder Southern Ocean SST. The extent of non sea-salt sea spray (using Ca^{2+} as a proxy; see Fisher and 28 other authors, 2007) relates to the extent of sea ice in the Indian Ocean sector which is paralleled with the northward shift in the SAF towards Australia. In contrast, in the Subantarctic Zone of the central South Pacific Ocean, the percentages of lithics recovered by Lamy et al. (2014) in core PS75/59-2 (Fig. 3F) displays a similar pattern as in our cores with substantial deposition of lithics during the period from 30 to 18 ka, with intermittent reduction of aeolian deposition over the core site between 21 and 20 ka and to a lesser extent at ~23 ka. On the other hand, the pre-30 ka record in that core is very different from the other records mentioned above suggesting aeolian transport in the central south Pacific Ocean over the period of 70 to 40 ka, except for a peak of (airborne) lithics in core PS75/59-2 that coincides with the peaks of dust (both Ti and quartz) in core 2611 (Fig. 3D). The low-resolution record of sea-ice diatoms in core SO136-111 (Crosta et al. (2004) SW of New Zealand at 56°40′S; see Fig. 3E) also indicates a significant decrease in sea-

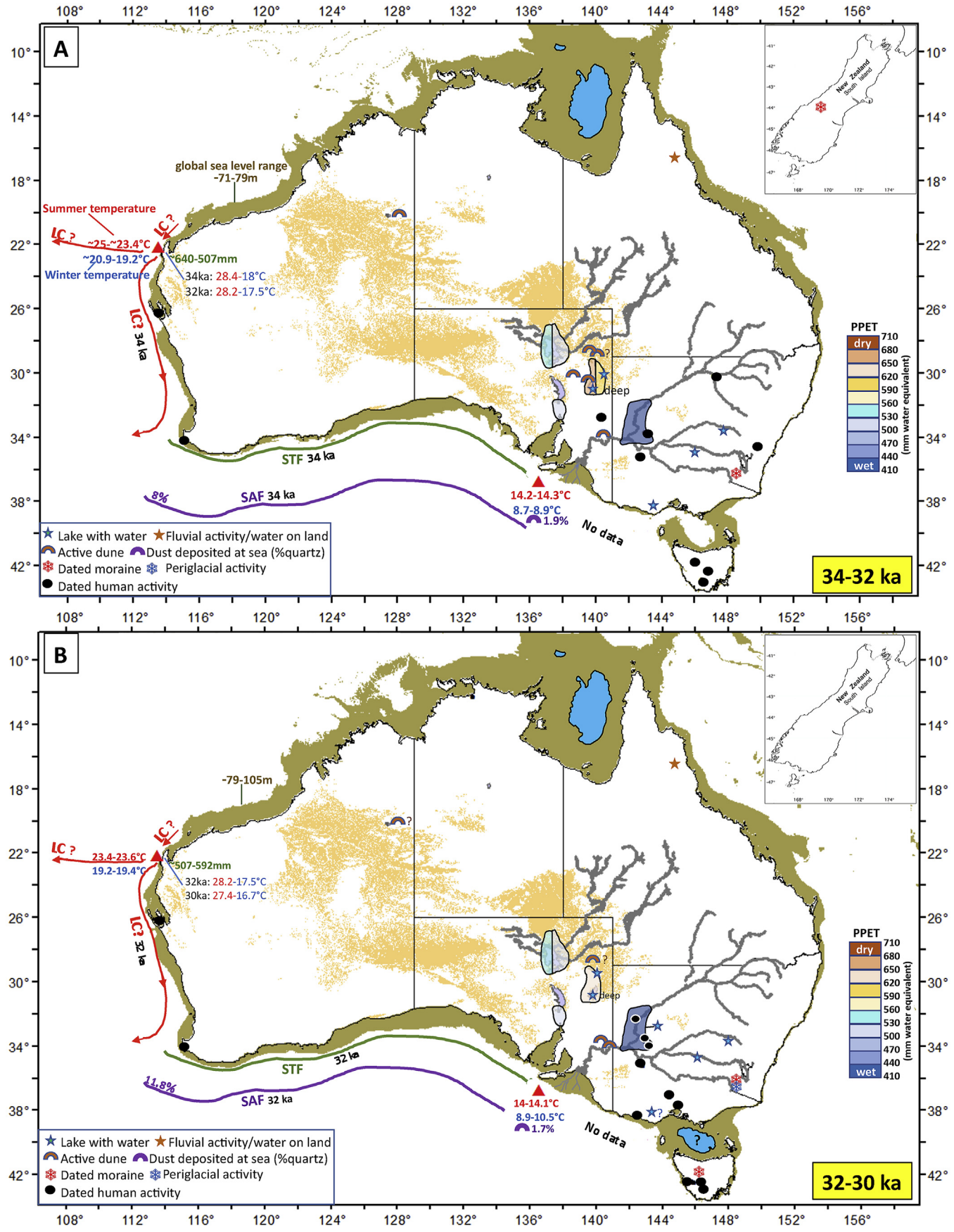
A
global sea level range
-71-79m
Summer temperature
LC ?
~25-~23.4°C
~20.9-19.2°C
Winter temperature
~640-507mm
34ka: 28.4-18°C
32ka: 28.2-17.5°C
LC? 34 ka
STF 34 ka
SAF 34 ka
8%
14.2-14.3°C
8.7-8.9°C
1.9%
No data
deep
PPET
dry
wet
710
680
650
620
590
560
530
500
470
440
410
(mm water equivalent)
Lake with water
Fluvial activity/water on land
Active dune
Dust deposited at sea (%quartz)
Dated moraine
Periglacial activity
Dated human activity
34-32 ka
B
-79-105m
LC ?
23.4-23.6°C
19.2-19.4°C
507-592mm
32ka: 28.2-17.5°C
30ka: 27.4-16.7°C
LC? 32 ka
STF 32 ka
SAF 32 ka
11.8%
14-14.1°C
8.9-10.5°C
1.7%
No data
deep
32-30 ka

Fig. 7. Maps of Australia, its coastline, rivers, dune fields and selected lacustrine sites, and the surrounding oceans summarising past environmental conditions for the 34 to 14 ka BP period, in time series spanning 2000 years. **(A)** for 34-32 ka; **(B)** 32-30 ka; **(C)** 30-28 ka; **(D)** 28-26 ka; and **(E)** 26-24 ka; **(F)** 24-22 ka; (**G)** 22-20 ka, including SST isotherms from Barrows and Juggins (2005); **(H)** 20-18 ka; **(I)** 18-16 ka; and **(J)** 16-14 ka. For each map, the position of sea level was taken from Lambeck et al. (2014) with the range listed with the value on the left (right) related to the oldest (youngest) age. Sea-surface temperatures (SST) (see text) are presented as follows: in red (blue) are summer (winter) temperatures, with the temperature on the left (right) related to the oldest (youngest) age span. The same convention is used for the land temperatures (using the same colour scheme for distinguishing between seasons) that were estimated from the occurrence of pollen assemblages in core Fr10-95/GC17 (van der Kaars and De Deckker, 2002, 2003); also the range of estimated mean annual land precipitation near Exmouth based on pollen data from the same core is presented in green. The tentative position of the Leeuwin Current (LC, in red) and the Subtropical Front (STF, in green) and Subantarctic Front (SAF, in mauve with percentages of subpolar foraminifera species also listed), all based on specific foraminifer assemblages, are shown. Data on ranges of point potential evapotranspiration for February plus March [PPET] in mm per water equivalent were taken from Miller et al. (2016a,b) for four different regions (see text for more information and ranges listed in the left legend) are presented. Note that at times 2 or 3 colours are shown for an area because of changes over the 2000 year period. Dated sites with evidence of human activity taken from the AustArch database (Williams et al., 2014) are shown by a black dot; dated evidence of aeolian activity were taken from different sources (see Supplementary Table 5 for more information) and are shown by a brown arch. Mauve arches refer to the presence of aeolian dust recovered in core 2611, with values for quartz percentages provided. A red (blue) asterisk relates to the evidence of glaciation (periglacial activity) (for both Australia and the South Island of New Zealand (insert at the top right-hand corner)). A blue star indicates a substantial site with water (see Supplementary Table 5 for more information). The presence of Lake Carpentaria is shown at the top of the map (based on De Deckker et al. (1988) and Reeves et al. (2007), as well as the tentative location of Bass Lake that would have been disconnected from the sea when sea level had fell below 67 m (see Blom (1988), Blom and Aslop (1988), and Jennings (1958) for historical information).

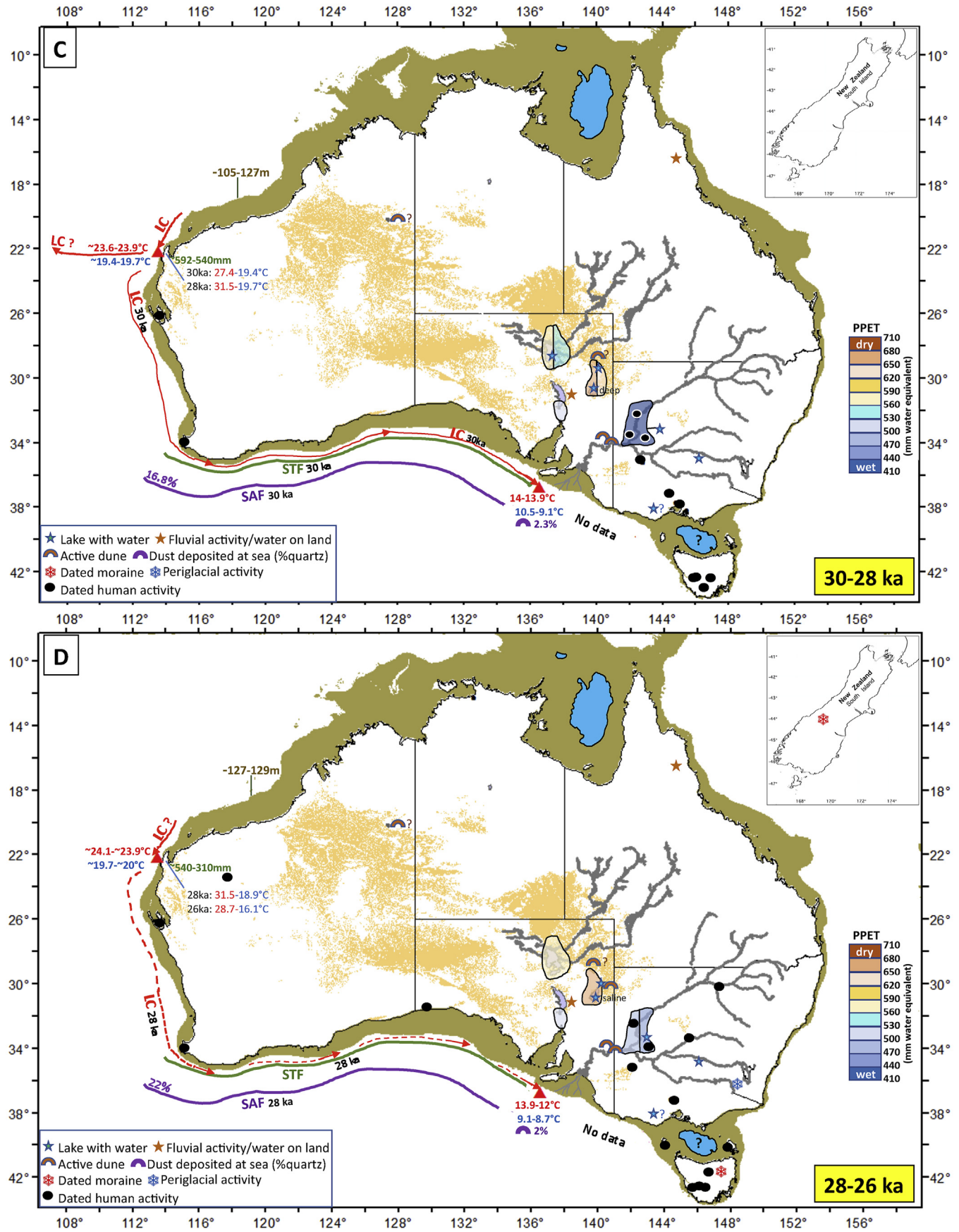

Fig. 7. (*continued*).

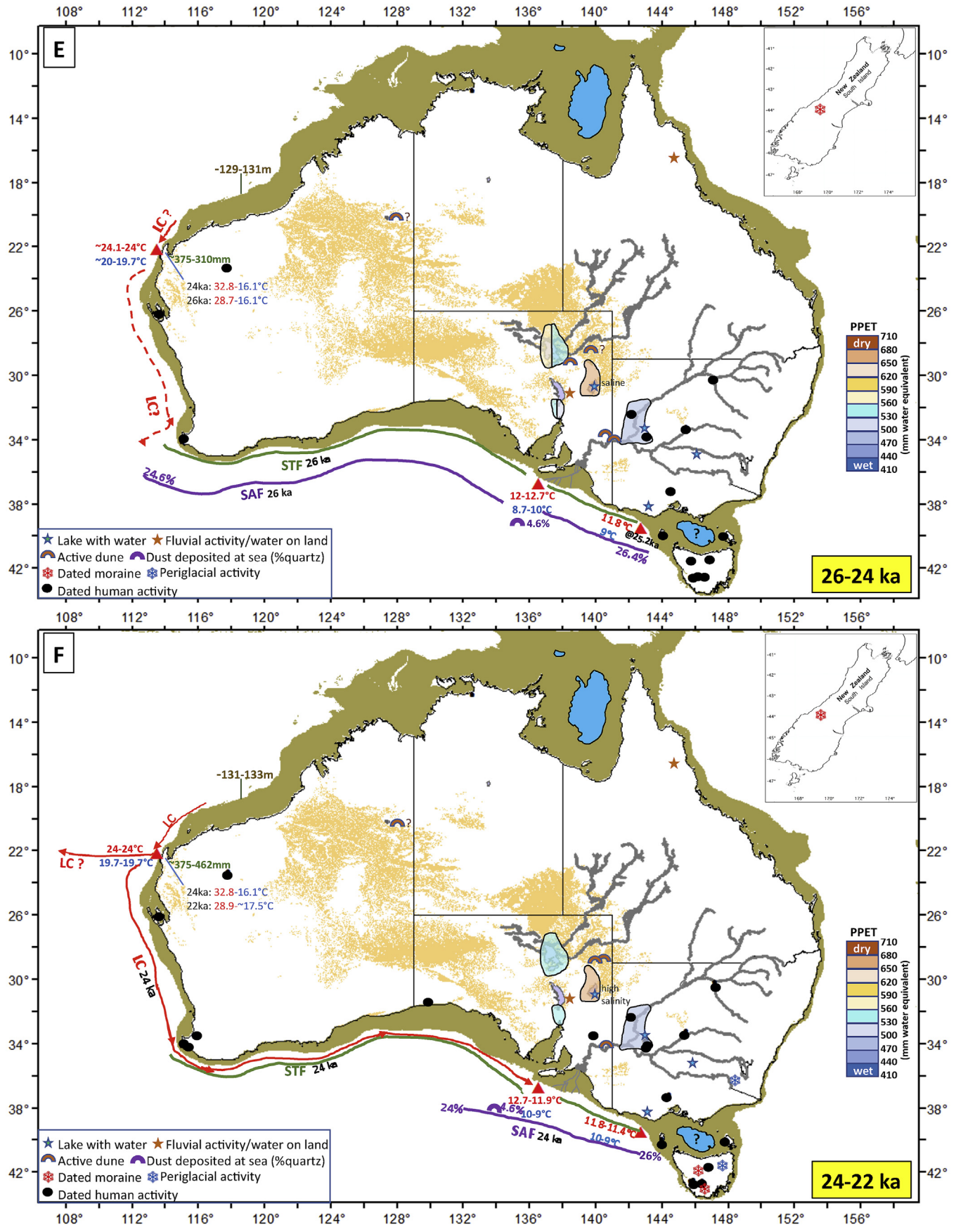

Fig. 7. (*continued*).

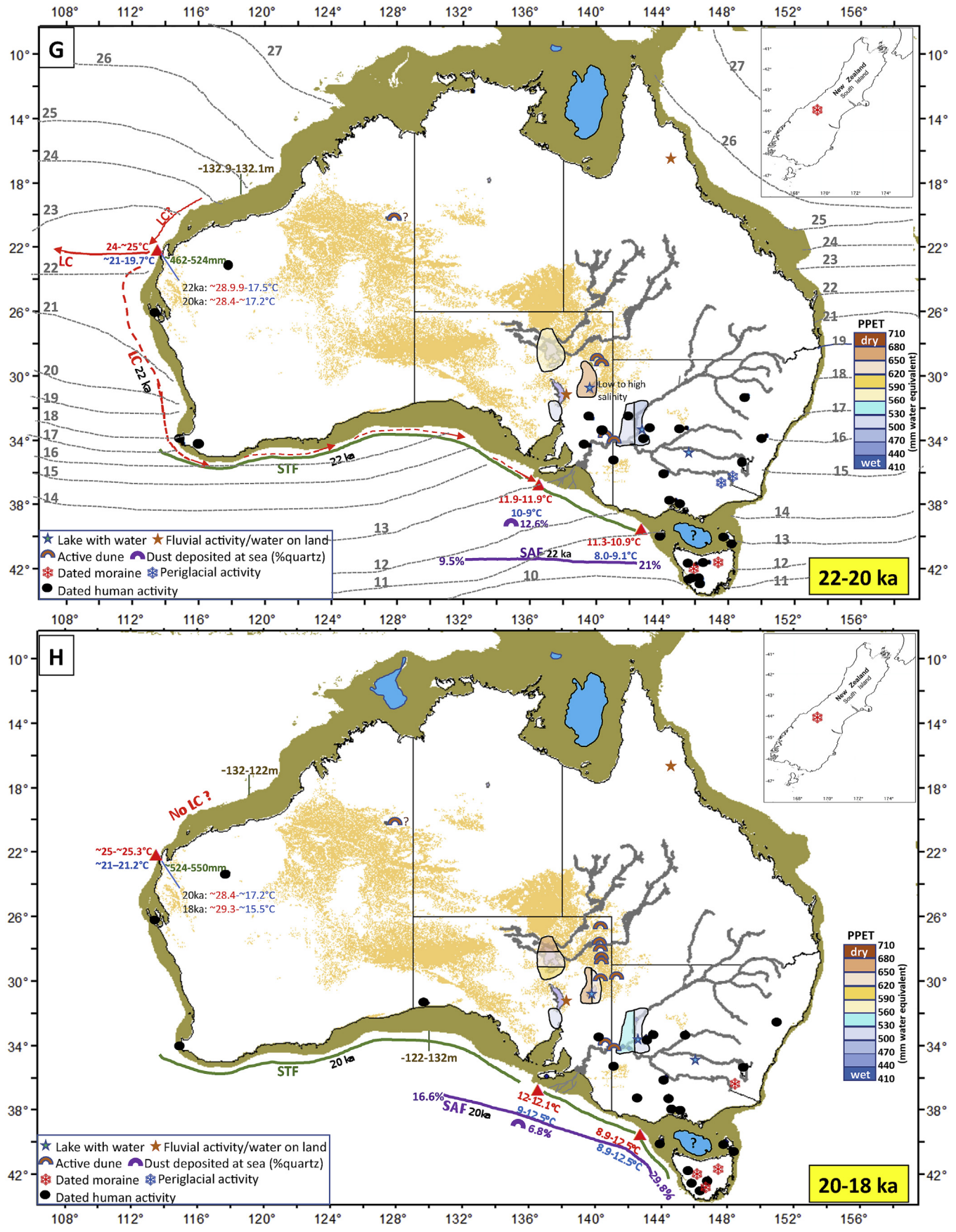

Fig. 7. (*continued*).

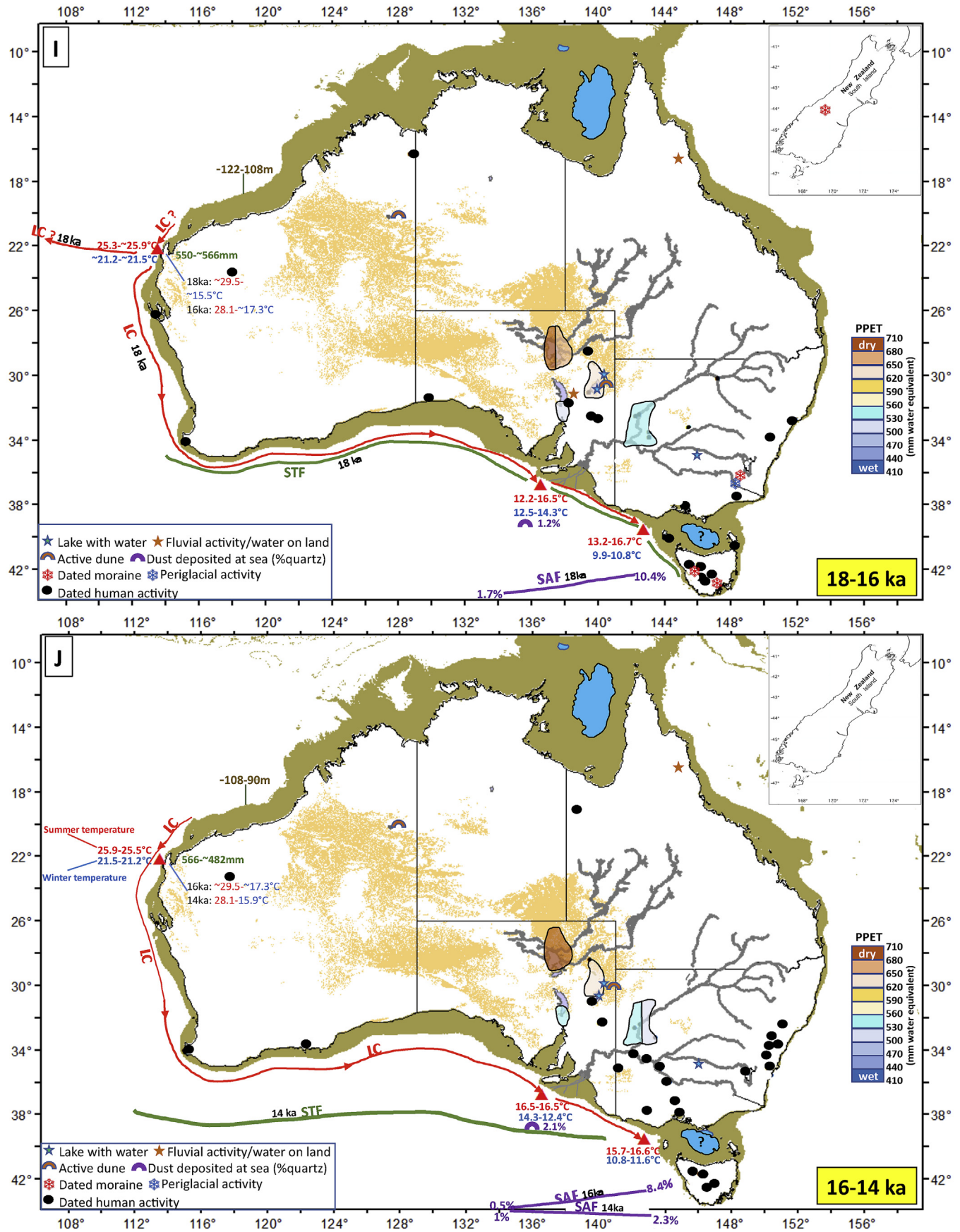

Fig. 7. (*continued*).

ice influence after 18 ka, at least SW of New Zealand. It is also noteworthy that sea-ice was prevalent during the period of 67 to 18 ka paralleling the high lithics transport in the SE Pacific (Lamy et al., 2013). The last 15 ka of the foraminiferal assemblages record in core 2611 indicates a stratified ocean (e.g. with little change in thermocline structure) with a reduced sea ice and a retreat of the SAF away from Australia.

Both temperature as well as methane increase significantly after 18 ka BP, with a return to low values for methane during the Antarctic Cold Reversal. The examination of the temperature and CH_4 stack records of Antarctic ice cores (taken from Parrenin et al. (2013) and Köhler et al. (2017), respectively) as shown in Fig. 4A and B displays significant increases of CH_4 as well as after 18 ka BP, with a return to low values for CH_4 during the Antarctic Cold Reversal. The CH_4 record shows many extensive high frequency fluctuations, many of which occur during HS5. There are no significant shifts in CH_4 during the 27 to 18 ka period when dust deposition at core site 2611 (Fig. 3D) or non sea-salt spray (=nss Ca^{2+}) at EPICA Dome C (Fig. 3A) were clearly important, even for the previous period of nss Ca^{2+} for the 32-29 ka period (Fisher and and 28 other authors, 2007).

6.2. The crysophere records of Australian and the South Island of New Zealand

Exposure dating using cosmogenic isotopes, has been used widely to date moraines in Australia (Fig. 1) and New Zealand. The record of ages are graphically presented in Fig. 3C with black squares representing ^{10}Be ages obtained from several localities in the South Island of New Zealand (Putnam et al., 2010, 2013a,Putnam et al., 2013b; Kelley et al., 2014; Doughty et al., 2015; Shulmeister et al., 2010, 2019a, b; Strand et al., 2019; Williams, 1996, Williams et al., 2010; Barrows et al., 2007), grey squares based on ^{36}Cl and some ^{10}Be ages for the Snowy Mountains (Barrows et al., 2001, 2002), and pale blue squares for Tasmania and based on ^{10}Be ages (Barrows et al., 2002), and a grey square for the pooled ^{36}Cl age for periglacial activity in Australia (Barrows et al., 2004).

Supplementary Figure 8 summarises the chronologies for the three regions against the percentage of *subpolar foraminifer species*. Supplementary Figure 8B shows a good correspondence with the timing of glaciation in Tasmania for most periods of the record when the Southern Ocean was colder, in particular for the period 28 to 18 ka. Nearly all exposure ages in New Zealand for various valleys coincide with periods of low SST (Supplementary Figure 8C), with the youngest ages coinciding with the ACR (Putnam et al., 2010; Supplementary Figure 8C).

In New Zealand where extensive dating campaigns were conducted - based on ^{10}Be isotopic chronologies - nearly all exposure ages for various valleys coincide with periods of low SSTs (Supplementary Figure 8C). We note also that the youngest New Zealand dates coincide with the ACR, as already established by Putnam et al. (2010) (Supplementary Figure 8C).

6.3. The Willandra Lakes record of western New South Wales

The interconnected lakes in the Willandra chain provides important information on human occupancy in association with waterbodies that would have provided ample food to humans. Humans were already present in the area by 50-46 ka and human burials have been dated to 40 ± 2 ka (Bowler et al., 2003). For the period, covering 55 to 17 ka, lake levels fluctuated with a series of dry lake phases (Bowler et al., 2012; Barrows et al., 2020). Supply of water to the arid zone at this time was controlled by more effective runoff associated with colder temperatures and therefore less evaporation (Barrows et al., 2020). Nevertheless, due to the reduced temperatures inland, evaporation must have been lower accordingly.

6.4. Records of lakes and fluvial activity in Australia

A number of sites, especially in eastern and South Australia provide evidence of the presence of water for the period that encompasses the glacial period. The presence of water must have been extremely important for human occupancy. Unfortunately, many of those records have poor chronologies. The best example being Lake George in eastern Australia, with a relatively small catchment (945 m^2), that has a documented record of lake filling, with beach ridges indicating lake levels up to 36 m deep (Coventry, 1976), with a pollen record (Singh and Geissler, 1985) and ostracods from the same core (De Deckker, 1982), but the radiocarbon chronology is in need of revision, with some dates obtained on soil carbonates that would have undergone pedogenic processes. Nevertheless, there is clear evidence that a permanently fresh waterbody was established around the LGM but the timing of this event remains unclear (see De Deckker, 2020).

Another important lake is Lake Carpentaria, now submerged below the Gulf of Carpentaria which today is ~65 m deep (Figs. 1, 6A-E). During periods of low sea level, it was cut off from the ocean and a very large lake (~300 × 600 km) formed (see Fig. 9 in Reeves et al., 2007). De Deckker et al. (1988) were the first to identify the timing and extent of the lake which had fresh to very low salinity water during the LGM. Reeves et al. (2007, 2008) studied a longer core taken in the Gulf near the depocentre of the lake and confirmed De Deckker et al.'s (1988) early palaeoenvironmental reconstructions for a lake dating from ~40 to 12 ka. Of interest is that during the LGM, the lake sediments were continuously laminated, pointing out that this area had not been affected by cyclonic activity (in contrast to today when cyclones frequently cross the Gulf) that would otherwise mix sediment in shallow water and destroy any lamination.

There are several other records of small lakes, marshes and swamps that indicate the presence of water during various periods of the last glacial, but they will not be discussed here as they are very regional, have very small catchments or are affected by the groundwater table. Further information on these sites are discussed in Turney et al. (2006) and Reeves et al. (2013).

6.5. Inland temperatures during the last glacial period

In 1965, Galloway presented an argument that during the glacial period in eastern Australia temperatures were lowered by at least 9 °C for the warmest month, based on observations of solifluction slopes in the Australian Alps. The figures estimated by Galloway (1965) in his early paper implied that glacial evaporation would have been significantly reduced, thus contributing to more water in the landscape. Using an independent line of evidence, Miller et al. (1997) determined the temperature-dependent amino acid racemization reaction rate from numerous dated fossil emu egg shell fragments from the interior of Australia. These authors calculated the change of racemization rate for low altitude, subtropical Australia for the period of 45 to 16 ka and estimated average air temperatures were at least 9 °C lower (see Miller et al., 1997's Fig. 2 with data that suggest that the temperature drop would have resulted from a reduction in atmospheric water vapour content).

Colhoun et al. (1999) established that the climate was colder at all times during the Last Glacial Stage until after ca. 14 ka BP using a pollen record from Lake Selina in western Tasmania. They also stated that the maximum temperature difference with MIS2 was

>3.5 °C. For a review of Tasmanian temperature changes, refer to Colhoun and Shimeld (2012) which mentions other temperature reconstructions based on pollen assemblages.

Based on pollen recovered from core tops taken offshore NW Western Australia and southern Indonesia, van der Kaars and De Deckker (2003) developed a transfer function that enabled De Deckker et al. (2014) to estimate both land temperatures and rainfall estimates (calculated by S. van der Kaars) for core Fr10/95-GC17 located close to Exmouth (Fig. 1). In the same paper, T.T. Barrows estimated SST using the modern analogue technique and planktic foraminifera. Some of the results from this paper are presented in Fig. 6 A-E and listed in Supplementary Table 5.

6.6. Regional evapotranspiration in Australia

There are several lines of evidence on evapotranspiration from Australia that are worthy of comparison with the information obtained from the deep-sea cores discussed earlier in this paper. Miller et al. (2016a,b) presented an extensive data set of $\delta^{18}O$ preserved in *Dromaius* (emu) fossil egg shell fragments from a near-continuous time series from central-southern Australia. The combined data provide independent reconstructions of climate over the past 100 ka. (Miller et al., 2016) which determined that the average $\delta^{18}O$ of sub-modern (<3 ka) *Dromaius* egg shells collected from 21 different localities (10–20 different eggshell at each locality) plotted against the contemporary February March (being Austral summer) PPET, in mm water equivalent) (see Fig. 6 in Miller et al., 2016; note that in the discussion below the NW Cape region will not be discussed further because the data showed significant outliers compared to the rest of the data). This enabled Miller et al. (2016a,b) to estimate PPET for the regions listed where fossil egg shells were collected and consequently dated. In conclusion, these authors stated that based on *Dromaius* egg shell $\delta^{18}O$, (1) all records show relatively moist conditions prior to 60 ka, with limited variability, and (2) peak aridity occurred in the regions between 30 and 15 ka, but showed no evidence of exceptional climate change between 60 and 40 ka. Miller et al. (2016a,b) reconstructed a time-series of PPET for the 5 regions and then computed a 20-point running means of $\delta^{18}O$ (refer to their Fig. 28 plotting the PPET for the five regions). These values were replotted here in Fig. 6A–D against time (0–95 ka) and plotted against SST for core 2611. Note the correlation between the records for the four regions, and in particular for the entirety of the record for the Lake Frome region (Fig. 6A) – with low PPET values - against the period spanning MIS4 that shows low SST. This correlation implies low evaporation and wet conditions coinciding with cool temperatures offshore southern Australia. The possible reason being that for the period of 50 to 20 ka see (Miller et al., 2016, Fig. 9), the isoleucine epimerization (A/I between 0.6 and 0.5) from KT-LE showed fairly similar values for the shells dated for the interval of 50 to 20 ka. This will require further scrutiny.

7. 34 to 14 ka in 2000-year time slices

This section documents events that occurred between 34 and 14 ka in the Australian region. After an initial rise after MIS4, SST slowly and steadily declined (Fig. 2B and C), except for rises coinciding with HS3 and HS4 in the Northern Hemisphere, culminating in a minimum during the LGM at ~18 ka BP. Mix et al. (2001) provided a definition of the LGM as *'chronologic, based on ages 19-23 cal-kyr BP (Chronozone level 1), or 18-24 cal-kyr BP (Chronozone level 2)'*. This was further refined by Clark et al. (2009), who reviewed the LGM and stated that ice sheets were at their maximum positions between 26.5 ka to 19 to 20 ka. Clark et al. (2009) based their observations on knowledge of sea level changes directly affected by the behaviour of the cryosphere. Clark et al. (2009) went on further to say that *"there is considerable regional variability in the timing of when ice sheets (and various sectors of ice sheets) first reached their local last glacial maxima (LLGM)"*. Clark et al. (2009)'s definition of the LGM is a revision of the EPILOG meeting's decision to define the LGM based on the global sea level minimum that spanned the period 23-19 ka (Mix et al., 2001). The MARGO project that followed on from EPILOG also used this definition (Barrows and Juggins, 2005; Kucera et al., 2005; MARGO project members, 2009). The use of the term "last glacial maximum", and in particular as applied to the Australian region, is in need of clarification, as several authors have used it differently such as in several of the OZ-INTIMATE publications: 23-18 ka (Turney et al., 2006); 21 ± 3 ka (Reeves et al., 2013); 22-18 ka (Petherick et al., 2013); start not defined but ends at 18 ka (Fitzsimmons et al., 2013). None of these authors in fact quote a source for their definition and then further added that nearly all ice sheets remained at their maximum position from 26.5 ka until 20-19 ka.

With the detailed study of Lambeck et al. (2014) dealing with sea level and global ice volumes from the Last Glacial Maximum to the Holocene, an attempt here is made to produce maps for the Australian region showing the periphery of Australia in ten reconstructions spanning the period of 34 to 14 ka each spanning two millennia (Fig. 7A–J). This 20,000 years interval was selected as it covers not only the extent of the LGM and also the deglaciation that followed. Data used in these maps are presented in Supplementary Table 5 divided into marine proxies (Supplementary Table 5A), land proxies (Supplementary Table 5B), lake level and related salinities (Supplementary Table 5C), including dated evidence of major fluvial activity, and dates for evidence of aeolian activity (Supplementary Table 5D). The bathymetric data used for producing the maps relies on the Australian Bathymetry and Topography Grid available from Geoscience Australia, and the coastal margins were constructed using the sea level estimates of Lambeck et al. (2014).

Before examining these maps, it is necessary to know that, for each time slot, some variables changed considerably. Therefore, examination of the original data sets stored at the www.pangaea.de website is warranted (refer to publications listed at the bottom of Supplementary Table 5).

No information on past vegetation is reproduced on these maps (refer the OZ-INTIMATE summary papers by Turney et al. (2006), Petherick et al. (2013), Reeves et al. (2013). A review by Kemp et al. (2019) of hydroclimate reconstructions covers the period covering Marine Isotopic Stage 3. Note that the palaeoceanographic reconstruction on the ten maps does not take into account data from several deep-sea cores where there are insufficient dates, or the sampling intervals are too coarse to warrant comparison with our cores. Some of the findings for these cores will be discussed in sections 7.1–7.10 below.

Also shown on Fig. 7A–J are sites in Australia from which dates of human occupation are available. This information was taken from the AustArch geochronological database of archaeological sites in Australia compiled by Williams et al. (2014). Out of 5522 records listed in the database for up to 2014, only 1089 were selected because they related directly to evidence of human occupation at those sites and span the 34 to 14 ka interval. Radiocarbon dates were calibrated using IntCal13 (Reimer et al., 2013) Note that the errors mean it is possible that the age overlaps two time slots. Nevertheless, these calibrated ages provide a good approximation of the location of human activity in Australia for the 34 to 14 ka period.

Finally, we will also use exposures age for glaciers and periglacial activity in Australia and New Zealand as the baseline for

determining environmental changes for the period. The reader is referred to Fig. 7 A-J, Fig. 8 and Supplementary Table 5 for each time slot. Variables presented in these sections are ordered from oldest to youngest on all the maps. For example, 12-10° indicates a decrease of 2 °C over the time slot. Note that values for the oldest time period are always presented on the left.

7.1. The 34-32 ka period (Fig. 7A)

Sea level fell from −71 (34 ka) to −79 m (32 ka) compared to today (Lambeck et al., 2014). There was a brief glaciation in the Snowy Mountains (Barrows et al., 2001) as well as on the South Island of New Zealand (Putnam et al., 2013a,Putnam et al., 2013b) and SSTs are moderately high both offshore Kangaroo Island (summer: 14.4°-14.2 °C; winter: 8.7°-8.9 °C) and NW Cape (summer: 25°-~23.4 °C, winter: 20.9°-19.2 °C) but winter SSTs are overall low. Coinciding with the glacial conditions on land, the SAF and STF are positioned closer to the southern coast of Australia (compared to today) - with 8% polar foraminifer taxa at 34 ka and increasing a little to ~12% at 32 ka, and the LC is absent in that area at this time. The STF is likely to be very close to the southwestern tip of Western Australia as the LC must not have passed that point; the westerlies may therefore have been located further north.

Suggested land temperatures varied much onshore near Exmouth (summer: 28.2-27.4; winter: 17.5–16.6 °C). Several lakes with relatively high levels, including the crater Lake Keilambete in western Victoria. PPET values along the lower Darling River are low, indicated relatively wet conditions. The other 3 regions studied by Miller et al. (2016a,b) show much considerable variation in PPET, with the Lake Frome area registering drier conditions, despite the fact that Lake Callabonna held water (Cohen et al., 2011, 2015). There was also much aeolian activity in the Strzelecki Desert (Fitzsimmons et al., 2007). In the north, Lake Carpentaria held water (Reeves et al., 2007, 2008) and the Fitzroy River catchment registered sporadic bedload transport (Croke et al., 2011); this is confirmed by estimated high rainfall by van der Kaars and De Deckker (2003), but eventually dropping ~20% near Exmouth (from 640 to 507 mm over two millennia). Northern Australia was therefore rather wet compared to the present.

We note that there was documented human occupation in Tasmania and along several tributaries of the Murray-Darling Basin (MDB), plus along the western coast of Western Australia. There was ample evidence of human occupation in northern Australia before 34 ka, (Williams et al. (2014)'s AustArch database; Clarkson et al. (2017, 2018), Hiscock (2017)), and also in the Willandra Lakes region (refer to Bowler et al., 2003, 2012).

7.2. The 32-30 ka period (Fig. 7B)

Sea level fell further, >20 m over the two millennia (Lambeck et al., 2014) to reach −105 m by 30 ka. Offshore Kangaroo Island, SST varied little both in summer and winter. Offshore NW Cape, SST remained almost unchanged within the limits of error. The percentage of subpolar species at site 2611 increased to 12% at 32 ka, suggesting a progressive northward shift of the SAF close to the Australian coast and, by analogy, the STF would have been almost bordering the coast at 32 ka. The percentage of *G. ruber* increased with 8% indicating a sporadic intrusion of the LC along the southern Australian coast by 30 ka. This is in contrast with subpolar foraminifera species becoming quite high by 30 ka (17%). In the Northern Hemisphere, Heinrich Stadial 3 was in force.

Glaciation continued into this interval in the Australian Alps (Barrows et al., 2001) and perhaps in the Tasmania (Barrows et al., 2002), but not on the South Island of New Zealand.

Rainfall increased near Exmouth and land temperatures remained almost unchanged for both seasons. Lake Carpentaria held water and the Fitzroy fluvial system in northern Queensland registered sporadic bedload transport (Croke et al., 2011). PPET estimates for the four regions by Miller et al. (2016a,b) remained unchanged except for the Lake Frome region became slightly drier, and there is fluvial activity in the Flinders Ranges (Williams et al., 2001). Wet conditions are noted along the tributaries of the River Murray, and the crater Lake Keilambete held water. Aeolian activity in the Strzelecki Desert was reduced (Fitzsimmons et al., 2007). Finally, there were more human occupation sites along the Darling River's tributaries and in south central Victoria, but in Tasmania the number of sites remains similar as for the previous two millennia.

7.3. The 30-28 ka period (Fig. 7C)

Sea level fell even further, by well over 20 m again over the two millennia (Lambeck et al., 2014) to reach −127 m by 28 ka. This is matched by a <1 °C SST drop in winter and almost no change in summer SSTs offshore Kangaroo Island and the percentage of subpolar foraminifera species eventually increased up to 22% by 28 ka and the *G. ruber* percentage progressively fell, indicating the waning influence of the LC, to almost inexistent at the end of this period.

Mean annual rainfall near Exmouth progressively fell, whereas land temperatures during both seasons decreased quite substantially, to the order of 10 °C. Further south, Kati Thanda-Lake Eyre held water early on and the Lake Frome region experienced an increase in PPET (meaning drier conditions) despite evidence of lakes in the region holding water. The same applies for the Willandra lakes in the vicinity of which there was ample evidence of human occupation.

Despite the progressive decrease in SST offshore Kangaroo Island, there is no evidence of glacial activity in the Australian region.

7.4. The 28-26 ka period (Fig. 7D)

Sea level was relatively unchanged only down to 130 m. Offshore Kangaroo Island SSST fell by almost 2 °C, but winter remained almost unchanged. The LC was almost non-existent and the SAF was further north near the southern Australian coast with 25% subpolar species by 26 ka. SST_{min} at the end of this period was at the lowest point at 9 °C. There is evidence of glacial activity on the South Island of New Zealand (Putnam et al., 2013b, 2013a; Doughty et al., 2015), but not in Australia.

At the northwestern corner of Australia near Exmouth, there was a dramatic drop in annual rainfall towards the end of this period (43%), but surprisingly SST increased a little during both seasons. It is no surprise therefore to see drier conditions (shown by PPET increases) in the Kati Thanda-Lake Eyre Basin and the Frome Basin, with some aeolian activity north of the latter. There is evidence of water at Lake Frome and in the Flinders Ranges. The Willandra lakes region held some water (Bowler et al., 2012; Barrows et al., 2020) and human activity is noted as well as in the northern part of the Darling sub-basin. There is also one human occupancy site in northwestern Western Australia and another in the Nullarbor Plain, as well as on both major islands in Bass Basin.

7.5. The 26-24 ka period (Fig. 7E)

Once more, sea level remained almost at the same low level but fell a further 2 m, only marginally down to −131 m. Being located further south, core GC15 registers a slightly higher percentage of subpolar foraminifer species (26%) at 25.2 ka (the oldest age recorded in that core). There was glacial activity in the South Island of New Zealand (Shulmeister et al., 2010, 2019a, b; Barrows et al.,

2013). There was ample aeolian activity in the Strzelecki Desert (Fitzsimmons et al., 2007) and in the western Murray Basin (Lomax et al., 2011). Aeolian activity in central and southern Australia remained almost unchanged because deposition of aeolian quartz at core site 2611 was 4.6% (at 26 ka) to 4.2% 2 ka later, and Ti influx at site 2611 increased a little. However, the significant change was the retreat of the SAF from Australia at site 2611 with a decrease from 25 to 7% in subpolar taxa, and in parallel the increase of *G. ruber* from 2 to 8%. The LC appeared to once again reach the site. The ocean bordering southern Australia was warming up and this may explain the absence of active glaciers in the Snowy Mountains on mainland Australia. Near Exmouth, annual rainfall progressively increased, summer land temperatures eventually increased by ~4 °C, but winter temperature remained unchanged. PPET signals remained almost the same as before for the four regions studied by Miller et al. (2016a,b). Evidence of human activity remained almost the same as for the previous period with no significant increase in dated sites.

7.6. The 24-22 ka period (Fig. 7F)

Sea level fell further to eventually reach −132 m (Lambeck et al., 2014). At 24 ka, the LC flowed along the southern coast of Australia but stopped short of core site 2611, and had almost vanished by 22 ka. By then, the SAF had moved northward near Kangaroo Island, but remained very close the Victorian coast (core site GC15) with 21% subpolar foraminifer species. Note that the highest value reached (since 34 ka) that occurred at 24 ka was 26%. SST continued to drop at site 2611 for both seasons, but remained almost unchanged at core site GC15 over the two millennia. There is evidence of glaciation in Tasmania in two areas, plus periglacial activity. Glaciation continued on the South Island of New Zealand. During this cold phase, aeolian dust levels significantly increased at site 2611 with 12.6% of quartz at 22 ka, up from to 4.4% at 24 ka. PPET levels showed increased wet conditions except for the Frome region. In NW Western Australia, rainfall increased by >20% and inland summer temperatures near Exmouth decreased by ~4 °C to the opposite of winter temperature increased by > 1 °C. Offshore Exmouth, summer and winter SST remained unchanged over the two millennia. Evidence of human activity remained almost the same as for the previous period with no significant increase in dated sites.

7.7. The 22-20 ka period (Fig. 7G)

Sea level remained in the vicinity of −133 m, with the lowest level recorded for the last glacial/interglacial cycle at ~ -134 m for a short period between 20.6 and 2.54 ka (Lambeck et al., 2014). The LC may have sporadically reached the 2611 site at 22 ka but had vanished by 20 ka. It did not reach site GC15 during those two millennia. The SAF definitely moved northward to site 2611 by 20 ka with 16% subpolar taxa ka but comparatively was even closer to the Victorian coast (at 30%). Summer SST was significantly lower at site 2611, with the lowest value (12 °C) recorded at 20 ka; SST_{min} remained unchanged from the previous two millennia (~9 °C). At core site GC15, SST during both seasons was lower, being located further south. Regional SST was at a minimum at this time (Barrows and Juggins, 2005). These low temperatures coincide with glacial activity in Tasmania and the South Island of New Zealand, and periglacial activity in the Australian Alps. During this cold period, PPET values indicate drier conditions, except for the Willandra lakes region where human activity was recorded (Bowler et al., 2003, 2012). The Nullarbor site is 'vacant' as well as the one in northern Western Australia, despite the fact that annual rainfall increased over time by ~12%. Lake Frome retained water but it was quite saline (De Deckker et al., 2010). Offshore Exmouth, both summer and winter SSTs may have increased by 1 °C but there are relatively few data points. There is an increase of dated human sites overall. Included on Fig. 7G are the mean SST contours produced by Barrows and Juggins (2005) which relate to the 21 ± 2 ka time interval. This gives an estimate of SST at 27 core sites located within the boundaries of our map. For further details, refer to Fig. 4b in Barrows and Juggins (2005).

7.8. The 20-18 ka period (Fig. 7H)

Sea level increased by 10 m to reach −122 m by 18 ka (Lambeck et al., 2014). The LC did not flow at 20 ka but strongly returned by 18 ka with *G. ruber* reaching 12% at site 2611. SST for both seasons and at both southern sites contrasted over the two millennia: almost unchanged in summer at site 2611 and ~2 °C at site GC15, and ~3.5 °C at site 2611 but <1 °C at site GC15. At 20 ka, there is evidence of glacial activity in the Australian Alps, several sites in Tasmania and in the South Island of New Zealand. Dry conditions prevailed in both the Kati Thanda-Lake Eyre and Frome regions, in contrast to Lake Mungo which held water only at the beginning of this period (Barrows et al., 2020) and the Port Augusta coastal sites of Miller et al. (2016a, b). There is evidence of extensive aeolian activity in the Strzelecki Desert (Fitzsimmons et al., 2007) but there is also a significant decrease of aeolian quartz deposited at site 2611. In NW Western Australia, near Exmouth, annual rainfall increased slightly, whereas land temperatures in summer increased by close to 1 °C whereas the reverse occurred in winter. Offshore SST for both seasons remained steady. The number of dated human sites increased overall near rivers in the SE corner of Australia, and humans returned to the Nullarbor and north-central Western Australia.

7.9. The 18-16 ka period (Fig. 7I)

Sea level continued to rise to eventually reach −108 m at 16 ka (Lambeck et al., 2014) and this coincided with dramatic SST increases at the southern core sites: in summer by > 4 °C at site 2611 and 3.5 °C at GC15; SST_{min} at both sites increased (~2° at 2611 and ~1 °C at GC15). By 16 ka, the percentages of *G. ruber* are very high (26% at 17.5 ka, 24% at 17.75 ka, and 23% at 16.8 ka, with fluctuations in between) and over the last 94 ka (Fig. 2E) at site 2611. To the east at site core site GC15 located some 600 km to the east, *G. ruber* reached 12% at 17.5 ka (Fig. 2E, Supp. Fig. 6). Offshore Exmouth, SSTs for both seasons remained almost unchanged, whereas inland summer temperatures fell by > 1 °C and winter temperature increased by < 2 °C; annual rainfall only increased slightly. Glaciers in the Snowy Mountains retreated to their last stillstand at 16 ka (Barrows et al., 2002). The supply of aeolian quartz progressively decreased from 5.7 to 1.2% quartz and this coincides with less aeolian activity in central Australia. Evidence of human occupation through dated sites (Williams et al., 2014) increased in eastern NSW and the south-central part of South Australia, with also one site in northern Australia.

7.10. The 16-14 ka period (Fig. 7J)

Sea Level continued to rise of the order of 18 m by 14 ka to eventually reach a level of −108 m. The LC would have continued to reach site 2611 despite decreased *G. ruber* percentages. Summer SST at site 2611 remained almost unchanged, whereas winter SST fell by ~2 °C. At site GC15, summer SSTs were almost identical to those at site 2611 but SST_{min} was ~3 °C lower. This probably indicates that the SAF was the furthest away from both sites during this 2 ka interval. The deposition of aeolian quartz at core site 2611

was low overall, but slightly higher at 14 ka, and this is paralleled by the decrease in active dunes east of Lake Frome with PPET values indicating somewhat dry conditions, with water still in that basin. By contrast, the Kati Thanda-Lake Eyre region was very dry as indicated by high PPET values. All the glaciers had vanished during this period. Evidence of human occupation through dated sites (Williams et al., 2014) increased further in southeastern Australia.

8. Discussion

8.1. The last 94 ka of climatic evolution in the Australian region and comparison with other cores

Our new well-dated cores provide high-resolution reconstructions that build on previous work in the region that are listed in supplement section 4.

8.2. Conditions in cores MD03-2611 and SS0206-GC15 related to glacial conditions on land

It is already clear that several environmental conditions determined from the study of our cores do not coincide with the period of lowest sea level (see reconstruction by Lambeck et al., 2014) and plotted in the following figures: Fig. 8A shows the plot of SST for cores 2611 and GC15 spanning the period of 30 to 17 ka. Unfortunately, the record of GC15 only commences at 25 ka. Nevertheless, the records show a rapid rise of SST in the vicinity of 18.7–18.6 ka (note that there is no estimate in core 2611 at 18.7 ka), and this is followed by a temperature rise of ~2.5–3 °C within less than 300 years (Fig. 8A). There is a maximum SST difference in both cores of ~9 °C with the middle of the Holocene (Figs. 2C and 4D). This is the same order of magnitude determined by Miller et al. (1997) for inland Australia and by Galloway (1965) for eastern Australia. In addition, Supplement fig. 7 shows that SST estimated for both cores using AUSMAT-F4 shows the same change in the vicinity of 18.7–18.6 ka. This is almost coincident with the timing of glaciation

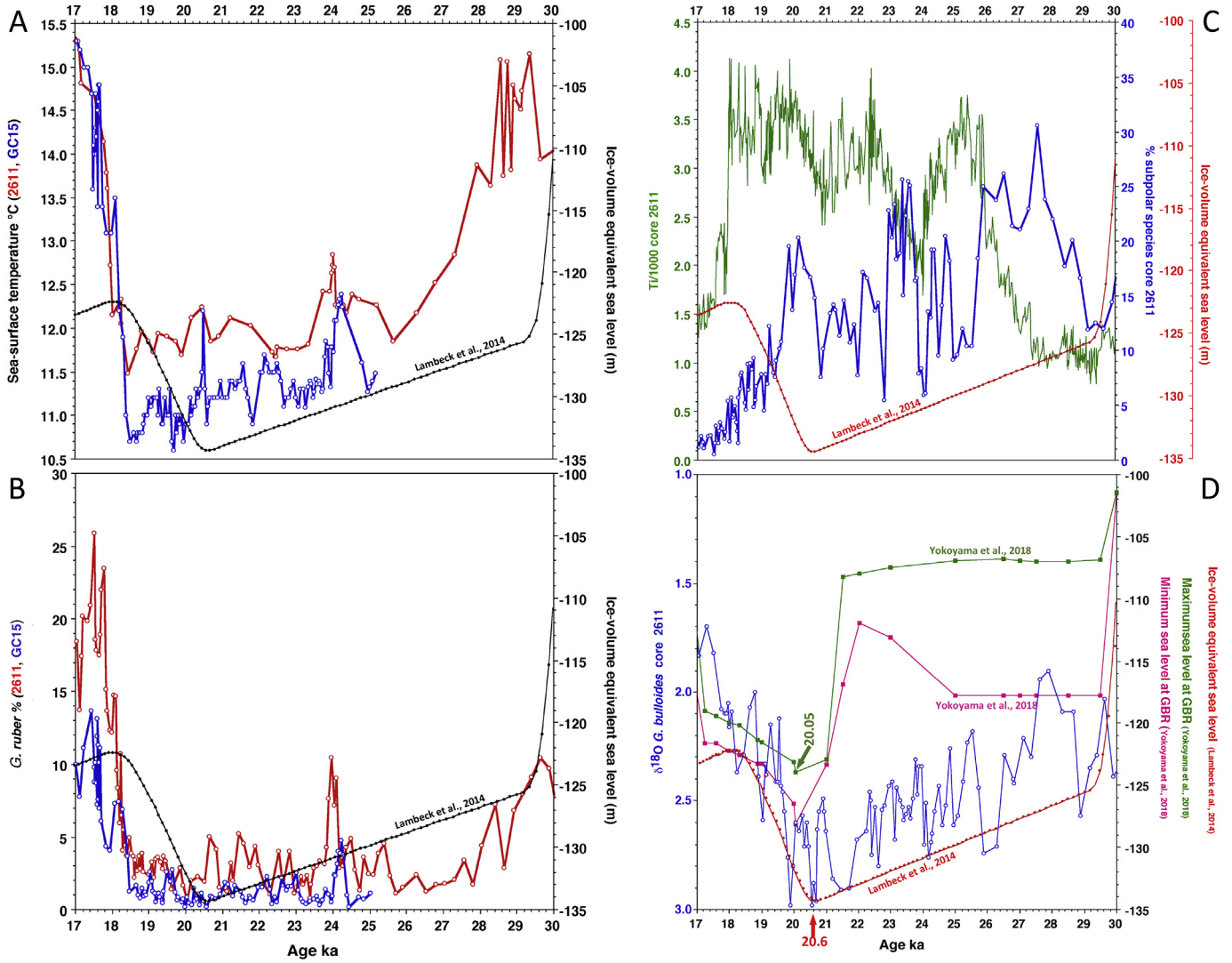

Fig. 8. Plots of selected records from deep-sea cores 2611 and GC15 against sea level from Lambeck et al. (2014) (shown in red or black) for the period of 30 and 17 ka BP.**A:** alkenone SST for core 2611 (in red) and core GC15 (in blue) versus age in ka BP. **B:** percentage of the subtropical foraminifer *G. ruber* indicative of the Leeuwin Current above the two core sites 2611 (in red) and GC15 (in blue); **C:** percentage of the subpolar foraminifera from core 2611 (in blue); also plotted is Ti (10 point running mean) indicative of aeolian dust deposited over the core site; **D**:δ^{18}O of *G. bulloides* of core 2611 (blue) and the sea level reconstructions for the Great Barrier Reef obtained by Yokoyama et al. (2018) with maximum levels in green and minimum levels in pink. The global sea level curve of Lambeck et al. (2014) appears in red.

in Australia. The New Zealand data point to a slightly older age for the complete deglaciation to have occurred on the South Island: 17.3 ± 0.5 ka for the Moana (Barrows et al., 2013); 17.84 ± 0.24 ka for the Rakaia inner most moraines with additional dates for ice-marginal moraines and ice-moulded bed rock dated as young as 15.66 ± 0.16 (Putnam et al., 2013b); 17.38 ± 0.51 ka for recessional moraines at Lake Ohau (Putnam et al., 2013a); 17.7 ± 0.3 ka, 17.74 ± 0.24 ka and 18.02 ± 0.15 ka for the Rangitata Glacier (Barrell et al., 2019). Also, the youngest ^{10}Be-dated innermost LGM moraines at Big Ben have an age of 17.84 ± 0.24 ka BP, whereas ice-marginal moraines or ice-moulded bedrock have ages of 17.02 ± 0.07, 17.1 ± 0.11, 16.96 ± 0.37, 16.25 ± 0.34, and 15.66 ± 0.16 ka BP, respectively (Putnam et al., 2013a, 2013b). A later age might be expected since the South Island of New Zealand is located further south than the two cores studied here.

SST began to decrease after 28 ka, but reached low values by 26 ka and SST_{min} from core 2611 decreases earlier at ~29 ka (Fig. 8A). Interestingly, SST fluctuated of the order of ~1 °C during the period of 26 to ~18.6 ka. It is also worth pointing out that the ice-volume equivalent sea level changes presented by Lambeck et al. (2014), with the lowest sea level around 20.6 ka are independent of local SST (Fig. 8A). The percentage of the LC indicator *G. ruber* is presented in Fig. 8B. Extremely low values in the most southerly located core (GC15) occurred from 24.4 ka until 18.6 ka, whereas they were overall slightly higher in core 2611 but started falling shortly before 28 ka. Importantly, in both cores, a significant shift is seen in both cores at ~18.6 ka that signals the arrival of the LC offshore Kangaroo Island and the western Victorian coast. Supplementary Figure 8 plots the percentage of subpolar foraminifera species for core 2611 against exposure ages for moraines (A: Tasmania, B: Snowy Mountains, and C South Island of New Zealand).

Fig. 8C compares the aeolian record from core 2611 and the percentage of subpolar species indicating changes in temperature and the position of oceanic fronts over the same core site (see also Supplementary Figure 9) which examines two principal proxies obtained from both cores (2611 and GC15): Titanium (as Ti/1000 cps, pink for 2611, green for GC15) plotted against the percentages of the subpolar foraminifera species, assuming that high percentages of the latter would indicate the proximity of the SAF to the southern coast of Australia (see also Fig. 7A–J). The progressive southward shift of the SAF commenced after 20 ka above core site 2611 and a millennium later above the GC15 core site. Finally, by 18.4 ka, the SAF had finally receded when the LC's influence was registered at both sites (compare Fig. 2E and Supplementary Figure 9). Examination of the earliest appearance of the SAF at core site 2611 suggests a northward shift after 29 ka which lasted about three millennia. The SAF again regained influence after 24 ka above core site 2611 and a few centuries earlier at the GC15 core site.

The provenance and climatic significance of aeolian dust at both core sites appears more complex, with the possibility of the airborne dust originating from different sources on the Australian continent (Fig. 8C; Supplementary Figure 9). The aeolian dust at site 2611 increased at 24 ka and possibly earlier at the GC15 site. Nevertheless, dust deposition at both core sites decreased rapidly at the same time between 18.4 and 18.2 ka (Supplementary Figure 9) while the LC extended over the sites (Fig. 2E). Eventually, dust deposition decreased to almost zero by 15 ka. Finally, there is no direct correlation between sea level change, SST and dust deposition at these sites (compare diagrams in Fig. 8 A-C).

To sum up, the commencement of post-glacial warming in the southern Australian region, and the southeastern Indian Ocean bordering it, is rapid after 18.6 ka coincident with the arrival of the LC and a drop in aeolian dust deposition. Glaciers persisted after this in the Snowy Mountains and Tasmania, with four moraines in the Snowy Mountains falling within that age range (Barrows et al., 2001, 2002), plus 12 in Tasmania (Barrows et al., 2002). On the other side of the continent, Sniderman et al. (2019) determined that SW Western Australia was essentially a treeless shrubland between 28 and 18 ka.

Conditions at the beginning of the LGM are somewhat less clear due to the time-transgressive signals from the two cores that are located on different latitudes, but by 24 ka cold SST and dust deposition had begun. We note also that water was present in the Willandra chain of lakes during this period. Hence, arid conditions were not ubiquitous in Australia and this permitted the presence of humans inland in special locations.

On the South Island of New Zealand, pooled ^{10}Be ages for moraines for the Ohau glacier returned an age of 27.4 ± 1.3 ka and for the Pukaki glacier an age of 27.17 ± 0.68 ka (Doughty et al., 2015) and 26.73 ± 0.74 ka BP (Strand et al., 2019). At Tekapo, Kelley et al. (2014) obtained a moraine age of 25.2 ± 0.7 ka BP. The presence of advanced glaciers clearly points to a broad regional cooling in the Australasian region. We argue that the strong stratification recognized in core 2611 by the large ($\Delta\delta^{18}O$ (*G. ruber-G. bulloides*, for the period of ~27-19 ka BP seen in core 2611 (Fig. 2A) that coincided with the northerly shift of the SAF implies that the westerlies belt could have shifted much further north than postulated by Toggweiler et al. (2006; Fig. 11) and Kohfeld et al. (2013), who suggested an equatorward shift of the maximum westerlies by approximately 3–5° latitude. Instead, we wish to argue here that in fact the westerlies belt could have been located over the Australian mainland. Hesse et al. (2004) in their review of Late Quaternary conditions and climates of the Australian arid zone, indicated Simpson Desert linear dunes near Finke had a significant deviation from modern source-bordering dune directions as identified by Nanson et al. (1995). Previously, Sprigg (1979, 1982) had calculated strong deviations of dune orientations near Lake Frome and further south which Hesse et al. (2004) assert were the result of local phenomena. Nevertheless, the westerlies during the LGM would have been some 3° further north compared to today over the Tasman Sea (Hesse et al., 2004). This was also supported by Martinez (1994) who showed a northerly shift of the Tasman Front of the same order of latitudinal magnitude; the position of this Front is obviously affected by winds and the Subtropical Ridge above it (Hesse, 1994).

Finally, the record of aeolian dust sedimentation from Native Companion Lagoon on Stradbroke Island (Fig. 1) located at the near extreme eastern edge of the Australian continent by Petherick et al. (2009), shows a significant dust flux peak of approximately ~29 g $m^{-2}.yr^{-1}$ at 22 ka, well above the average range value of 1–8 g $m^{-2}.yr^{-1}$ for the entire record spanning 25 ka (see Fig. 11 in Petherick et al., 2009).

8.3. Comparison of the cooling maximum and global sea level

Lambeck et al. (2014) provided an outstanding data set combining high-resolution information on sea levels. Over ~1000 observations of localities worldwide far from former ice margins for the past 35 ka. A plot of these data for the period spanning 30 to 17 ka BP (Fig. 8) shows that the estimated sea level equivalent started to rise at 21.6 ka BP during the LGM, having reached a low of −134 m, after a slow decline from 29 to 21 ka (refer to Lambeck et al. (2014)'s Fig. 4A and B). The most positive $\delta^{18}O$ values in core 2611 occurred at ~21.7 ka BP for *G. ruber* and 20.6 and also at 19.9 ka BP for *G. bulloides* (Figs. 2A and 8D), possibly coinciding with the lowest sea level. However, this does not take into account temperature changes (which varied considerably during that time, see Fig. 2B and C) or salinity changes in the water mass. The global sea

level low and subsequent rise just after 21.6 ka BP occurs some 2 millennia before local SST started to rise (at 18.4 ka BP, see Fig. 2B and C, 8A). We note that by 18.4 ka BP, global sea level had already risen by some 11 m from the minimum at 20.6 ka (Lambeck et al., 2014). The start of the northern hemisphere melting of ice sheets is not 'immediately' transmitted in the Australian region and its surrounding oceans. Locally, on the Great Barrier Reef, Yokoyama et al. (2018) identified that sea level rose after 20.05 ka (Fig. 8D) and this is close the global ice-equivalent sea level data modelled by Lambeck et al. (2014). Of interest is that the highest $\delta^{18}O$ value recorded by *G. bulloides* is very close to the lowest sea level recorded by Yokoyama et al. (2018) on the Great Barrier Reef, even knowing that the isotopic record of foraminifera is affected by both salinity as well as water temperature.

8.4. Evidence of a major cold and wet event during MIS4

During MIS 4, SST decreased by 5 °C (Fig. 2B). Core 2611 records a maximum SST drop of close to 6 °C in the period spanning just after 71 ka until after 59 ka BP. (Fig. 2A). The foraminifera fauna changed in composition and in particular the subpolar taxa increase (Fig. 2E–J). The SST drop occurred at a much faster rate than the entry into LGM (Fig. 2). On the Australian mainland, Barrows et al. (2001) identified the Early Kosciuszko glaciation which consisted of a single glacier advance at 59.3 ± 5.4 ka BP coined the Snowy River Advance. There is also possible periglacial activity in the Victorian Highlands and Tasmania (Barrows et al., 2004) near the end of this interval. Schaefer et al. (2015) dated a glacier advance at 65.1 ± 2.7 ka on the South Island of New Zealand. Further evidence from New Zealand glaciers at this time comes from Shulmeister et al. (2010, 2019a, b), based on infrared stimulated luminescence dated the Acheron Bank in the Rakai Valley, and Williams (1996); Williams et al. (2010) for glaciofluvial sediments generated when the Aurora Cave was overrun by a glacier (see also Supplementary Figure 8).

Near or after the termination of MIS4, Cohen et al. (2011, 2015) interpreted high lake level phases at Lake Frome (Fig. 1) and a high level at Lake Callabonna to the north of Frome at 57.9 ± 3.1 ka. At Kati-Thanda-Lake Eyre, Magee et al. (2004) identified a similar high lake level (Phase III) with a mean pooled age of 63.5 ± 1.3 ka.

Bayon et al. (2017), who studied the Nd isotopic ratios of numerous samples from core 2607, has previously postulated that the filling of the megalakes Eyre and Frome during MIS4 resulted from the southern shift of the ITCZ that would have helped fill the Darling River sub-basin during that time. However, the puzzling feature is that the older high lake levels recorded at the 2 megalakes coincided with the filling of the Murray River sub-basin as shown by more negative εNd signatures (see Bayon et al., 2017). This remains at odds with the data for MIS4, as it implies rain reaching the Murray Darling Basin would have originated this time from the South.

8.5. Events postdating MIS4

In central Australia, Cohen et al. (2015) who dated palaeoshorelines and river deposits in the Lake Eyre Basin, determined that a final disconnection between Lakes Kati Thanda-Eyre and Frome occurred at 48 ± 2 ka BP leading to a progressive drop in the level of Lake Mega-Frome. These authors claim that this drying phase led to large scale aridification, and they further suggested that this coincided with the arrival of humans and the demise of the megafauna in Australia. In the recent study of deep-sea core MD03-2614, van der Kaars et al. (2018) determined the presence of the coprophilous spore *Sporormiella,* that is found on dung produced by herbivores which is considered to be a proxy for herbivore biomass (Davis and Shafer, 2006). van der Kaars et al. (2017) found a marked decline in the spores after 45 ka BP that indicates megafaunal population collapse, from 45 ka to 43.1 ka BP, well after the climate shift recognized in core 2611 (Figs. 2B and 4 D-F). However, there is a decrease of ~0.5 per mil in the *G. ruber* $\delta^{18}O$ record in core 2614 that coincides with the significant SST drop recorded in core 2611 during which time an even stronger positive shift in planktic $\delta^{18}O$ (Fig, 2A). In addition, Miller et al. (2016a,b), who discussed the extinction of the giant bird *Genyornis newtowni*, estimated that the continent-wide extinction of the megafauna must have occurred at 46.4 ka BP, but with a confidence interval of 51 to 40 ka BP based on OSL and U-series ages of articulated megafaunal remains at some 28 sites (see Roberts et al., 2001).

Finally, Bowler et al. (2003) re-evaluated dates for human activity and remains at Lake Mungo and established that humans were present at Mungo as early as 50–46 ka ago, when local lake levels were high. Bowler et al. (2003) established that artefacts were found between 2 gravel beds which were formed during high water level stands when the lake would have overflowed (see Fig. 3 in Bowler et al., 2003). These authors further indicated that fluctuations between lake-full and drier conditions existed after 55 ka BP that coincided with increases of dust deposition. The recent work by Barrows et al. (2020) that revisited the dating at Mungo confirms this wet phase with only one OSL age at 53.4 ± 3.1 ka BP during which time the lake may have held up to 9 m of water.

8.6. Climatic evolution in Australia and human occupation

It is pertinent now to examine the climatic context of human arrival and occupation in Australia. Humans obviously would have migrated around Australia where water was available, and examination of the ten maps (Fig. 7A–J) that encompass the LGM show that people were present in parts of Australia when conditions were much colder than today (~9 °C) as well as dry, with aeolian activity and deflation from lake and river overflow sites. However, it was not universally dry everywhere in southern Australia during the LGM. Some rivers yielded water as a result of melting of seasonal snow, especially in spring, such as postulated for the Willandra chain of lakes (Bowler et al., 2012; Barrows et al., 2020). The number of sites occupied increases with time (Fig. 7A–J and Williams et al., 2014). However, this may result of taphonomic/preservation bias. Veth et al. (2017) highlight the importance discontinuities of archaeological records in Australian north-western maritime deserts. It is clear from examination of the PPET information obtained by Miller et al. (2016a,b) information that during MIS4, Australia's centre as well as the Darling River region and near Port Augusta that precipitation was quite substantial, accompanied by less evaporation. There is now evidence of human presence from 65 ka BP in northern Australia (Clarkson et al., 2017; but see also related discussions in Dortch and Malaspinas, 2017; Veth, 2017; Hiscock, 2017; Wood, 2017; Clarkson et al., 2018; O'Connell et al., 2018) and it is no surprise therefore that humans occupied northern Australia, since we now have evidence that the ITCZ had migrated south over inland Australia (refer to discussion in the above section 8.4). It is likely also that humans occupied the shore of the large Lake Carpentaria when it was fresh (see Reeves et al., 2008, 2009). Obviously, marine archaeology would provide many answers to those suggestions (see discussions in Ward et al., 2018).

9. Conclusion

Based on the high-resolution record of deep-sea core 2611, spanning the last 94 ka, accompanied by the 25 ka record of nearby GC15, we have been able to document significant changes that occurred at the ocean surface. The potential position of oceanic

fronts and the presence of the subtropical Leeuwin Current over the core sites. was estimated for the 34-14 ka BP period. The occurrence of aeolian dust at the two core sites allowed us to determine the timing of dust production and, to some extent the aerial distribution of arid conditions on the adjacent land mass.

We review in great detail the environmental conditions during the LGM which occur in the study area from 24 to 18 ka BP. During that period, glaciers were active on the Australian mainland, Tasmania and New Zealand, SST and aeolian input fluctuated. This was accompanied by regional changes in latitude of isotherms and probably oceanographic fronts accompanied by atmospheric wind changes.

Two additional cold periods are highlighted in the cores: (1) the first being between ~50.5 ka and 48 ka BP, when SST decreased by ~6 °C and aeolian dust deposition increased, and (2) centred around 27 ka BP that coincides also with glacier advance in New Zealand, but not presently identified in the Australian region. After this period, warmer conditions ensued before the start of the coldest part of the LGM proper at ~24 ka BP in the cores.

Ten time slice maps, each covering a period of 2000 years for the period of 34 to 14 ka BP. These show selected published data from the Australian region with sound chronologies. These maps show the fluctuations of temperature along the southern margin of Australia as well as the extent of the Leeuwin Current (LC) which contributed to the transport of tropical heat from north of Australia. When the LC was absent along the southern coastline of Australia, we conclude that the southern westerlies belt was either stronger or had shifted northward and may have 'locked' the Subtropical Front against the southern tip of Western Australia. This scenario occurred during the LGM and the older cold periods. Interestingly, Gottschalk et al. (2019), who modelled shifts of the westerlies belt for the Southern Hemisphere concluded that a northward (southward) shift would induce an increase (decrease) in subsurface CO_2 therefore releasing (segregating) atmospheric CO_2 from the Southern Ocean. The occurrence of the foraminifer *G. bulloides* indicative of upwelling associated with frontal movements would be a good candidate for testing this hypothesis. However, it is not until we have a better age control in our cores spanning the last glacial/interglacial cycle relying on good estimates of the marine reservoir in the Southern Ocean through time, that we will be able to compare our core data with that of ice cores in Antarctica. The remaining complication is that if upwelling does occur the marine reservoir ages could modify accordingly.

During the LGM, mean annual SSTs in the cores located south of Australia were of the order of 9 °C colder than during for the mid-Holocene, similar to that in central Australia for the period from 45 to 16 ka BP. (Miller et al., 1997). This also supports estimates by Galloway (1965) based on periglacial deposits in the Snowy Mountains. Since the mid-Holocene, a progressive temperature drop of the order of 2 °C (Calvo et al., 2007; Lopes dos Santos et al., 2013 and data presented here), coincides with a progressive return to arid conditions as witnessed by a supply of aeolian dust at core site 2611 (Gingele et al., 2007).

Concerning MIS4, SSTs were low - of the order of 6 °C – during extensive glaciation existed on the South Island of New Zealand, and in the Snowy Mountains. In contrast, the February March (Austral summer) point-potential evapotranspiration in central Australia implied low evaporation and wet conditions suggesting a southern shift of the Intertropical Convergence Zone over Australia.

Finally, despite the original concept of Australia being arid and cold during the LGM, there is evidence for water availability in parts of the Australian continent, especially its northern part, as well as Tasmania, that helped sustain human activity. Obviously, there is no information on human activity along the submerged coastline of Australia but it is more than likely that the coastal zone would have nurtured more human activity during settlement this vast landmass.

Author contributions

PDD obtained the marine cores (MD03-2611, SO0206-GC15 and Fr10/95-CG17) and he supervised the processing of the cores. He also wrote the first draft of the paper to which all the co-authors contributed. MM organised, prepared and distributed many of the samples to various parties in Germany, Norway, Poland and Switzerland. He also carried out the XRD analyses on core 2611 as well as conducted the XRF analyses. He drew Figs. 2 – 5 together with PDD. KP counted all the foraminifer samples and interpreted the faunal assemblages with MM. LW prepared and interpreted many of the older radiocarbon dates done in core 2611. TB and RS carried out and interpreted the samples for alkenone palaeothermometry. MM modelled the chronology of both southern Australian cores. TTB calculated the SST based on KP's foraminifer data and also calibrated the radiocarbon ages used for plotting the human occupation sites on the 10 maps. He also commented on the contents of the penultimate draft of the manuscript. TO'L drafted the base maps used in Fig. 1 and Fig. 7 A-E on which PDD placed all the information. EJ provided stable isotope analyses and obtained funding for many of the ^{14}C analyses.

Data Availability

The new data presented in this paper are available at https://doi.pangaea.de/10.1594/PANGAEA.911846.

Declaration of competing interest

The authors declare that they have no known competing financial interests or personal relationships that could have appeared to influence the work reported in this paper.

Acknowledgements

Core MD03-2601 was obtained during the AUSCAN cruise funded by grants from the Australian Research Council (ARC), the ANU Faculty Research Fund and the National Oceans Office, all awarded to PDD. The skills of Yvon Balut in obtaining the core are gratefully acknowledged as well as the French Paul Emile Victor Polar Institute [IPEV] that gave PDD access to the *RV Marion Dufresne*. Core SS0206-GC15 was obtained during a *RV Southern Surveyor* cruise funded by grants from the ARC and the ANU Faculty Research Fund also awarded to PDD. Don McKenzie was of much help during that cruise and so were all its members. Parts of this work received funding from the European Research Council under the European Community's Seventh Framework Programme (FP7/2007–2013)/ERC grant agreement 610055 as part of the Ice2Ice project.

PDD is grateful to Dr Tim Cohen for providing ages for beach ridge changes in the Lake Frome-Callabonna area, and to Professor Sean Ulm for providing the AustArch database. PDD benefitted from discussion on New Zealand glacial chronologies with Professor George Denton, Emeritus Professor Paul Williams and Professor James Shulmeister.

We also benefited from the comments of two anonymous reviewers as well as from the editor Dr A. Voelker that helped improve the quality of the manuscript in a number of places and corrected us on the marine reservoir ages. Thank you all.

Appendix A. Supplementary data

Supplementary data to this article can be found online

at https://doi.org/10.1016/j.quascirev.2020.106593. https://doi.pangaea.de/10.1594/PANGAEA.911846.

References

Barrell, D.J.A., Putnam, A.E., Denton, G.H., 2019. Reply to comment received from J. Shulmeister et al. regarding "Reconciling the onset of deglaciation in the upper Rangitata valley, Southern Alps, New Zealand" (Quaternary Science Reviews 203 (2019), 141-150.). Quat. Sci. Rev. 219, 316–318.

Barrows, T.T., Almond, P., Rose, R., Fifield, L., Mills, S.C., Tims, S.G., 2013. Late Pleistocene glacial stratigraphy of the Kumara-Moana region, West Coast of South Island, New Zealand. Quat. Sc. Rev. 74, 139–159.

Barrows, T.T., Fitzsimmons, K.E., Mills, S., Turney, J., Pappin, D., Stern, N., 2020. Late Pleistocene lake level history of lake Mungo, Australia. Quat. Sci. Rev. 238, 106338.

Barrows, T.T., Juggins, S., 2005. Sea-surface temperatures around the Australian margin and Indian Ocean during the last glacial maximum. Quat. Sci. Rev. 24, 1017–1047.

Barrows, T.T., Juggins, S., De Deckker, P., Calvo, E., Pelejero, C., 2007. Long-term climate change in the Australian-New Zealand region. Paleoceanography 22, PA2215. https://doi.org/10.1029/2006PA001328.

Barrows, T.T., Stone, J.O., Fifield, L.K., Creswell, R., 2001. Late Pleistocene glaciation of the Kosciuszko Massif, Snowy Mountains, Australia. Quat. Res. 55, 179–189.

Barrows, T.T., Stone, J.O., Fifield, L.K., 2004. Exposure ages for Pleistocene periglacial deposits in Australia. Quat. Sci. Rev. 23, 697–708.

Barrows, T.T., Stone, J.O., Fifield, L.K., Creswell, R., 2002. The timing of the last glacial maximum in Australia. Quat. Sci. Rev. 21, 159–173.

Bayon, G., De Deckker, P., Magee, J.W., Germain, Y., Bermell, S., Tachikawa, K., Norman, M.D., 2017. Extensive wet episodes in Late Glacial Australia resulting from high-latitude forcings. Sci. Rep. 7 article 44054.

Bé, A.W.H., 1977. In: Ramsay, A.T.S. (Ed.), An Ecological, Zoogeographic and Taxonomic Review of Recent Planktonic Foraminifera. *Oceanic Micropaleontology*. Academic Press, London), pp. 1–100.

Bé, A.W.H., Tolderlund, D.S., 1971. In: Funnel, B.M., Riedel, W.R. (Eds.), Distribution and Ecology of Living Planktonic Foraminifera in Surface Waters of the Atlantic and Indian Oceans, The Micropalaeontology of the Oceans. Cambridge University Press, Cambridge, pp. 105–149.

Blom, W.M., 1988. Late Quaternary sediments and sea-levels in Bass Basin, southeastern Australia – a preliminary report. Search 19, 94–96.

Blom, W.M., Alsop, D.B., 1988. Carbonate mud sedimentation on a temperate shelf: Bass Basin, southeast Australia. Sediment. Geol. 60, 269–280.

Bowler, J.M., 1978. Glacial age aeolian events at high and low latitudes: a Southern Hemisphere perspective. In: van Zinderen Bakker, E.M. (Ed.), Antarctic Glacial History and World Palaeoenvironments. A.A. Balkema, Rotterdam, pp. 149–172.

Bowler, J.M., Gillespie, R., Johnston, H., Boljkovac, K., 2012. Wind v water: glacial maximum records from the Willandra Lakes. Terra Aust. 34, 271–296.

Bowler, J.M., Johnston, H., Olley, J.M., Prescott, J.R., Roberts, R.G., Shawcross, W., Spooner, N.A., 2003. New ages for human occupation and climatic changes at Lake Mungo. Nature 412, 837–840.

Broecker, W.S., 2002. Massive iceberg discharges as triggers for global climate change. Nature 372, 421–424.

Butzin, M., Heaton, T.J., Köhler, P., Lohmann, G., 2020. A short note on marine reservoir age simulations used in IntCal20. Radiocarbon. https://doi.org/10.1017/RDC.2020.9.

Calvo, E., Pelejero, C., De Deckker, P., Logan, G.A., 2007. Antarctic deglacial pattern in a 30 kyr record of sea surface temperature offshore South Australia. Geophys. Res. Lett. 34, L13707. https://doi.org/10.1029/2007GL029937.

Clark, P.U., Dyke, A.S., Shakun, J.D., Carlson, A.E., Clark, J., Wohlfarth, B., Mitrovica, J.X., Hostetler, S.W., McCabe, A.M., 2009. The last glacial maximum. Science 325 (5941), 710–714.

Clarkson, C., et al., 2017. Human occupation of northern Australia by 65,000 years ago. Nature 547, 306–310.

Clarkson, C., Roberts, R.G., Jacobs, Z., Marwick, B., Fullagar, R., Arnold, L.J., Hua, Q., 2018. Reply to comments on Clarkson et al. (2017) 'Human occupation of northern Australia by 65,000 years ago'. Aust. Archaeol. 84, 84–89.

Cohen, T.J., Nanson, G.C., Jansen, J.D., Jones, B.G., Jacobs, Z., Treble, P., Price, D.M., May, J.-H., Smith, A.M., Ayliffe, L.K., Hellstrom, J.C., 2011. Continental aridification and the vanishing of Australia's megalakes. Geology 39, 167–170.

Cohen, T.J., Jansen, J.D., Gliganic, L.A., Larsen, J.R., Nansen, G.C., May, J.-H., Jones Price, D.M., 2015. Hydrological transformation coincided with megafaunal extinction in central Australia. Geology 43, 195–198.

Colhoun, E.A., Shimeld, P.W., 2012. Late-Quaternary vegetation history of Tasmania from pollen records. Terra Aust. 34, 297–328.

Colhoun, E.A., Pola, J.S., Barton, C.E., Heijnis, H., 1999. Late Pleistocene vegetation and climate history of Lake Selina, western Tasmania. Quat. Int. 57/58, 5–23.

Coventry, R.J., 1976. Abandoned shorelines and the late Quaternary history of Lake George, New South Wales. J. Geol. Soc. Aust. 23, 249–273.

Croke, J., Jansen, J.D., Amos, K., Pietsch, T.J., 2011. A 100 ka record of fluvial activity in the Fitzroy River Basin, tropical northeastern Australia. Quat. Sci. Rev. 30, 1681–1695.

Croudace, I.W., Rindby, A., Rothwell, R.G., 2006. ITRAX: description and evaluation of a new multifunction X-ray core scanner. In: Rothwell, R.G. (Ed.), New Techniques in Sediment Core Analysis, vol. 267. Geological Society, London, Special Publication, pp. 51–63.

Crosta, X., Sturm, A., Armand, L., Pichon, J.-J., 2004. Late Quaternary sea ice history in the Indian sector of the Southern Ocean as recorded by diatom assemblages. Mar. Micropaleontol. 50, 209–223.

Davis, O.K., Shafer, D.S., 2006. *Sporormiella* fungal spores, a palynological means of detecting herbivore density. Palaeogeogr. Palaeoclimatol. Palaeoecol. 237, 40–50.

De Angelis, M., Traversi, R., Udisti, R., 2012. Long-term trends of mono-carboxylic acids in Antarctica: comparison of changes in sources and transport processes at the two EPICA deep drilling sites. Tellus B 64. https://doi.org/10.3402/tellusb.v64i0.17331.

De Deckker, P., 1982. Late Quaternary ostracods from Lake George, New South Wales. Alcheringa 6, 305–318.

De Deckker, P., 2020. The record of Weereewa - Lake George with an ambiguous dating issue. Quat. Australasia 37, 21–23.

De Deckker, P., Arnold, L.J., van der Kaars, S., Bayon, G., Stuut, J.-B.W., Perner, K., Lopes dos Santos, R., Uemura, R., Demuro, M., 2019. Marine Isotope Stage 4 in Australasia: a full glacial culminating 65,000 years ago – global connections and implications for human dispersal. Quat. Sci. Rev. 204, 187–207.

De Deckker, P., Barrows, T.T., Rogers, J., 2014. Land–sea correlations in the Australian region: post-glacial onset of the monsoon in northwestern Western Australia. Quat. Sci. Rev. 105, 181–194.

De Deckker, P., Chivas, A.R., Shelley, J.M.G., Torgersen, T., 1988. Ostracod shell chemistry: a new palaeoenvironmental indicator applied to a regressive/transgressive record from the Gulf of Carpentaria, Australia. Palaeogeogr. Palaeoclimatol. Palaeoecol. 66, 231–241.

De Deckker, P., Magee, J.W., Shelley, J.M.G., 2010. Late Quaternary palaeohydrological changes in the large playa Lake Frome in central Australia, recorded from the Mg/Ca and Sr/Ca in ostracod valves and biotic remains. J. Arid Environ. 75, 38–50.

De Deckker, P., Moros, M., Perner, K., Jansen, E., 2012. Influence of the tropics and southern westerlies on glacial interhemispheric asymmetry. Nat. Geosci. 5, 266–269.

Donders, T.H., Haberle, S.G., Hope, G., Wagner, F., Visscher, H., 2007. Pollen evidence for the transition of the Eastern Australian climate system from the post-glacial to the present-day ENSO mode. Quat. Sci. Rev. 26, 1621–1637.

Dortch, J., Malaspinas, A.S., 2017. Madjedbebe and genomic histories of Aboriginal Australia. Aust. Archaeol. 83, 174–177.

Doughty, A.M., Schaefer, J.M., Putnam, A.E., Denton, G.H., Kaplan, M.R., Barrell, D.J.A., Andersen, B.G., Kelley, S.E., Finkel, R.C., Schwartz, R., 2015. Mismatch of glacier extent and summer insolation in Southern Hemisphere mid-latitudes. Geology 43, 407–410.

Etourneau, J., Schneider, R., Blanz, T., Martinez, P., 2010. Intensification of the Walker and Hadley atmospheric circulations during the Pliocene–Pleistocene climate transition. Earth Planet Sci. Lett. 297, 103–110.

Fairbanks, R.G., Sverdlove, M., Free, R., Wiebe, P.H., Bé, A.W.H., 1982. Vertical distribution and isotopic fractionation of living planktonic foraminifera from the Panama Basin. Nature 298, 841–844.

Fisher, H., and 28 other authors, 2007. Reconstruction of millennial changes in dust emission, transport and regional sea ice coverage using the deep EPICA ice cores from the Atlantic and Indian Ocean sector of Antarctica. Earth Planet Sci. Lett. 260, 340–354.

Fitzsimmons, K.E., Rhodes, E.J., Magee, J.W., Barrows, T.T., 2007. The timing of linear dune activity from the Strzelecki and Tirari Deserts, Australia. Quat. Sci. Rev. 26, 2598–2616.

Fitzsimmons, K.E., Cohen, T.J., Hesse, P.P., Nanson, G.C., May, J.-H., Barrows, T.T., Haberlah, D., Hilgers, A., Kelly, T., Larsen, P., Lomax, J., Trebble, P., 2013. Late Quaternary palaeoenvironmental change in the Australian drylands. Quat. Sci. Rev. 74, 78–95.

Galloway, R.W., 1965. Late Quaternary climates of Australia. J. Geol. 73, 603–618.

Gingele, F.X., De Deckker, P., Norman, M., 2007. Late Pleistocene and Holocene climate of SE Australia reconstructed from dust and river loads deposited offshore the River Murray Mouth. Earth Planet Sci. Lett. 255, 257–272.

Gottschalk, J., 14 other authors, 2019. Mechanisms of millennial-scale atmospheric CO_2 change in numerical model simulations. Quat. Sci. Rev. 220, 30–74.

Grant, K.M., et al., 2012. Rapid coupling between ice volume and polar temperature over the last 150,000 years. Nature 491, 744–747.

Heinrich, H., 1988. Origin and consequences of cyclic ice rafting in the northeast Atlantic Ocean during the past 130,000 years. Quaternary Reearch 29, 142–152.

Hesse, P.P., 1994. The record of continental dust from Australia in Tasman Sea sediments. Quat. Sci. Rev. 13, 257–272.

Hesse, P.P., 2016. How do longitudinal dunes respond to climate forcing? Insights from 25 years of luminescence dating of the Australian desert dunefields. Quat. Int. 410, 11–29.

Hesse, P.P., Magee, J.W., van der Kaars, S., 2004. Late Quaternary climates of the Australian arid zone: a review. Quat. Int. 118–119, 87–102.

Hill, P., De Deckker, P., 2004. AUSCAN Seafloor Mapping and Geological Sampling Survey on the Australian Southern Margin by RV *Marion Dufresne* in 2003. Geoscience Australia Record 2004/04, p. 136 pp.

Hill, P., De Deckker, P., von der Borch, C.C., Murray-Wallace, C.V., 2009. The ancestral

Murray River on the Lacepede Shelf, southern Australia: late Quaternary migrations of a major river outlet and strandline development. Aust. J. Earth Sci. 56, 135–157.
Hiscock, P., 2017. Discovery curves, colonisation and Madjedbebe. Aust. Archaeol. 83, 168–171.
Ho, S.L., Mollenhauer, G., Lamy, F., Martínez-Garcia, A., Mohtadi, M., Gersonde, R., Hebbeln, D., Nunez-Ricardo, S., Rosell-Melé, Tiedemann, R., 2012. Sea surface temperature variability in the Pacific sector of the Southern Ocean over the past 700 kyr. Paleoceanography 27, PA4202. https://doi.org/10.1029/2012PA002317.
Jaeschke, A., Wengler, M., Hefter, J., Ronge, T.A., Geibert, W., Mollenhauer, G., et al., 2017. A biomarker perspective on dust, productivity,and sea surface temperature in the Pacific sector of the Southern Ocean. Geochim. Cosmochim. Acta 204, 120–139.
Jennings, J.N., 1958. The submarine topography of Bass Strait. Proc. Roy. Soc. Vic. 71, 49–71.
Kelley, S.E., Kaplan, M.R., Schaefer, J.M., Andersen, B.G., Barrell, D.J.A., Putnam, A.E., Denton, G.H., Schwartz, R., Finkel, R.C., Doughty, A.M., 2014. High-precision ^{10}Be chronology of moraines in the Southern Alps indicates synchronous cooling in Antarctica and New Zealand 42,000 years ago. Earth Planet Sci. Lett. 405, 194–206.
Kemp, C.W., Tibby, J., Arnold, L.J., Barr, C., 2019. Australian hydroclimate during Marine Isotope Stage 3: a synthesis and review. Quat. Sci. Rev. 204, 94–104.
King, A.L., Howard, W.R., 2003. Planktonic foraminifera flux seasonality in Subantarctic sediment traps: a test for paleoclimate reconstruction. Paleoceanography 18. https://doi.org/10.1029/2002PA000839.
Kohfeld, K.E., Graham, R.M., de Boer, A.M., Sime, L.C., Wolff, E.W., Le Quéré, C., Bopp, L., 2013. Southern Hemisphere westerly wind changes during the Last Glacial Maximum: paleo-data synthesis. Quat. Sci. Rev. 68, 76–95.
Köhler, P., Nehrbass-Ahles, C., Schmitt, J., Stocker, T.F., Fisher, H., 2017. A 156 kyr smoothed history of the atmospheric greenhouse gases CO_2, CH_4, and N_2O and their radiative forcing. Earth Syst. Sci. Data 9, 363–387.
Kucera, M., Schneider, R., Weinelt, M., 2005. MARGO – multidisciplinary approach for the reconstruction of the glacial ocean surface. Quat. Sci. Rev. 24 (7–9), 813–1107.
Lambeck, K., Rouby, H., Purcell, A., Sun, Y., Sambridge, M., 2014. sea level and global ice volumes from the last glacial maximum to the Holocene. Proc. Natl. Acad. Sci. Unit. States Am. 43 https://doi.org/10.1073/pnas.1411762111.
Lamy, F., Gersonde, R., Winckler, G., Esper, O., Jaeschke, A., Kuhn, G., Ullermann, J., Martinez- Garcia, A., Lambert, F., Kilian, R., 2014. Increased dust deposition in the Pacific Southern Ocean during glacial periods. Science 343 (6169), 403–407.
Lomax, J., Hilgers, A., Radtke, U., 2011. Palaeoenvironmental change recorded in the palaeodunefields of the western Murray Basin, South Australia - new data from single grain OSL-dating. Quat. Sci. Rev. 30, 723–736.
Lopes dos Santos, R., Spooner, M.I., Barrows, T.T., De Deckker, P., Sinninghe, J.S., Schouten, S., 2013. Comparison of organic (UK'37, TEXH86, LDI) and faunal proxies (foraminiferal assemblages) for reconstruction of late Quaternary sea surface temperature variability from offshore southeastern Australia. Paleoceanography 28, 1–11. https://doi.org/10.1002/palo.20035.
Mackintosh, A.N., Barrows, T.T., Colhoun, E.A., Fifield, L.K., 2006. Exposure dating and glacial reconstruction at Mt Field, Tasmania, Australia, identifies MIS3 and MIS2 glacial advances and climatic variability. J. Quat. Sci. 21, 363–376.
Magee, J.W., Miller, G.H., 1998. Lake Eyre palaeohydrology from 60 ka to the present: beach ridges and glacial maximum aridity: Palaeogeography, Palaeoclimatology. Palaeoecology 144, 307–329.
Magee, J.W., Miller, G.H., Spooner, N.A., Questiaux, D., 2004. Continuous 150 k.y. monsoon record from Lake Eyre, Australia: insolation-forcing implications and unexpected Holocene failure. Geology 32, 885–888.
Martinez, J.I., 1994. Late Pleistocene palaeoceanography of the Tasman Sea: implications for the dynamics of the warm pool in the western Pacific. Palaeogeogr. Palaeoclimatol. Palaeoecol. 112, 19–62.
May, J.-H., Barrett, A., Cohen, T.J., Jones, B.G., Price, D., Gliganic, L.A., 2015. Late Quaternary evolution of a playa margin at Lake Frome, south Australia. J. Arid Environ. 122, 93–198.
Middleton, J.F., Bye, J.A.T., 2007. A review of the shelf-slope circulation along Australia's southern shelves: Cape Leeuwin to Portland. Prog. Oceanogr. 75, 1–41.
Miller, G.H., Fogel, M.L., Magee, J.W., Gagan, M.K., 2016a. Disentangling the impacts of climate and human colonization on the flora and fauna of the Australian arid zone over the past 100 ka using stable isotopes in avian eggshell. Quat. Sci. Rev. 151, 27–57.
Miller, G.H., Magee, J.W., Jull, A.T.J., 1997. Low-latitude glacial cooling in the Southern Hemisphere from amino-acid racemization in emu eggshells. Nature 385, 241–244.
Miller, G.H., Magee, J.W., Smith, M., Spooner, N.J., Baynes, A., Lehman, S., Fogel, M., Johnston, H., Williams, D., Clark, P., Florian, C., Holst, R., DeVogel, S., 2016b. Human predation contributed to the extinction of the Australian megafaunal bird *Genyornis newtoni* by 47 ka. Nat. Commun. 7, 10496.
Mix, A.C., Bard, E., Schneider, R., 2001. Environmental processes of the ice age: land, oceans, glaciers (EPILOG). Quat. Sci. Rev. 20, 627–657.
Moros, M., De Deckker, P., Jansen, E., Perner, K., Telford, R.J., 2009. Holocene variability in the Southern Ocean recorded in a deep-sea sediment core off South Australia. Quat. Sci. Rev. 28, 1932–1940.
Moros, M., De Deckker, P., Perner, K., Ninnemann, U., Wacker, L., Telford, R., Jansen, E., Siegel, H., Blanz, T., Schneider, R., submitted 7 June 2020. Oceanic frontal shifts south of Australia linked to global atmospheric changes over the last deglaciation. Quat. Res..
Moros, M., McManus, J.F., Rasmussen, T., Kuijpers, A., Dokken, T., Snowball, I., Nielsen, T., Jansen, E., 2004. Quartz content and the quartz-to-plagioclase ratio determined by X-ray diffraction: a proxy for ice rafting in the northern North Atlantic? Earth Planet Sci. Lett. 218, 387–399.
Müller, P.J., Fischer, G., 2001. A 4-year sediment trap record of alkenones from the filamentous upwelling region off Cape Blanc, NW Africa and a comparison with distributions in underlying sediments. Deep-Sea Res. I 48, 1877–1903.
Müller, P.J., Kirst, G., Ruhland, G., von Storch, I., Rosell-Mele, B., 1998. Calibration of the alkenone paleotemperature index $U^{37'}_{K}$ based on core tops from the eastern southern South Atlantic and the global ocean (60°N-60°S). Geochem. Cosmochim. Acta 62, 1757–1772.
Nanson, G.C., Chen, X.Y., Price, D.M., 1995. Aeolian and fluvial evidence of changing climate and wind patterns during the past 100 ka in the western Simpson Desert, Australia. Palaeogeogr. Palaeoclimatol. Palaeoecol. 113, 87–102.
O'Connell, J.F., et al., 2018. When did *Homo sapiens* reach southeast Asia and Sahul. Proc. Natl. Acad. Sci. Unit. States Am. org/10.1073/pnas.1808385115.
Olley, J.M., De Deckker, P., Roberts, R.G., Fifield, L.K., Yoshida, C.H., Hancock, G., 2004. Optical dating of deep-sea sediments using single grains of quartz: a comparison with radiocarbon. Sediment. Geol. 169, 175–189.
Parker, F.L., 1962. Planktonic foraminiferal species in Pacific sediments. Micropaleontology 8, 219–254.
Parrenin, F., Masson-Delmotte, V., Köhler, P., Raynaud, D., Paillard, D., Schwander, J., Barbante, C., Landais, A., Wegner, A., Jouzel, J., 2013. Synchronous change of atmospheric CO_2 and Antarctic temperature during the last deglacial warming. Science 339 (6123), 1060–1063.
Pelejero, C., Calvo, E., Barrows, T.T., Logan, G.A., De Deckker, P., 2006. South Tasman Sea alkenone palaeothermometry over the last four glacial/interglacial cycles. Mar. Geol. 230, 73–86.
Perner, K., Moros, M., De Deckker, P., Blanz, T., Wacker, L., Telford, R., Siegel, H., Schneider, R., Jansen, E., 2018. Heat export from the tropics drives mid to late Holocene palaeoceanographic changes offshore southern Australia. Quat. Sci. Rev. 180, 96–110.
Petherick, L., Bostock, H., Cohen, T.J., Fitzsimmons, K., Tibby, J., Fletcher, M.-S., Moss, P., Reeves, J., Mooney, S., Barrows, T., Kemp, J., Jansen, J., Nanson, G., Dosseto, A., 2013. Climatic records over the past 30 ka from temperate Australia - a synthesis from the Oz-INTIMATE workgroup. Quat. Sci. Rev. 74, 58–77.
Petherick, L.M., McGowan, H.A., Kamber, B.S., 2009. Reconstructing late Quaternary dust transport pathways for eastern Australia using trace element composition of long traveled dusts. Geomorphology 105, 67–79.
Prahl, F.G., Wakeham, S.G., 1987. Calibration of unsaturation patterns in long-chain ketone compositions for palaeotemperature assessment. Nature 330, 367–369.
Putnam, A.E., Denton, G., Schaefer, J.M., Barrell, D.J.A., Andersen, B.G., Finkel, R.C., Schwartz, R., Kaplan, M., Schlüchter, C., 2010. glacier advance in southern middle-latitudes during the Antarctic cold reversal. Nat. Geosci. 3, 700–704.
Putnam, A.E., Schaefer, J.M., Denton, G.H., Barrell, D.J.A., and 11 other authors, 2013b. Warming and glacier recession in the Rakaia valley, southern Alps of New Zealand, during Heinrich stadial 1. Earth Planet Sci. Lett. 382, 98–110.
Putnam, A.E., Schaefer, J.M., Denton, G., Barrell, D.J.A., Birkel, S.D., Andersen, B.G., Kaplan, M., Finkel, R.C., Schwartz, R., Doughty, R., 2013a. The last glacial maximum at 44 degrees S documented by a Be-10 moraine chronology at Lake Ohau, southern Alps of New Zealand. Quat. Sci. Rev. 62, 114–141.
Reeves, J.M., Chivas, A.R., Garcia, A., De Deckker, P., 2007. Palaeoenvironmental change in the Gulf of Carpentaria (Australia) since the last interglacial based on Ostracoda. Palaeogeogr. Palaeoclimatol. Palaeoecol. 246, 163–187.
Reeves, J.M., Chivas, A.R., Garcia, A., Holt, S., Couapel, M.J.J., Jones, B.G., Cendon, D.I., Fink, D., 2008. The sedimentary record of palaeoenvironments and sea-level change in the Gulf of Carpentaria, Australia, through the last glacial cycle. Quat. Int. 183, 3–22.
Reeves, J.M., Barrows, T.T., Cohen, T.J., Kiem, A.S., Bostock, H.C., Fitzsimmons, K.E., Jansen, J.D., Kemp, J., Krause, C., Petehrick, L., Phipps, S.J., OZ-INTIMATE Members, 2013. Climate variability over the last 35,000 years recorded in marine and terrestrial archives in the Australian region: an OZ-INTIMATE compilation. Quat. Sci. Rev. 74, 21–34.
Reimer, P.J., Bard, E., Bayliss, A., Beck, J.W., Blackwell, P.G., Bronk Ramsey, C., et al., 2013. IntCal13 and MARINE013 radiocarbon age calibration curves 0-50000 year. Radiocarbon 55, 1869–1887.
Roberts, R.G., Flannery, T.F., Ayliffe, L.K., Yoshida, H., Olley, J.M., Prideaux, G.J., Laslett, G.M., Baynes, A., Jones, R., Smith, B.L., 2001. New ages for the last Australian megafauna: continent-wide extinction about 46,000 years ago. Science 292, 1888–1892.
Schaefer, J.M., Putnam, A.E., Denton, G.H., Kaplan, M.R., Birkel, S., Doughty, A.M., Kelley, S., Barrell, D.J.A., Finkel, R.C., Winckler, G., Anderson, R.F., Ninneman, U.S., Barker, S., Schwartz, R., Andersen, B.G., Schlüchter, C., 2015. The Southern Glacial maximum 65,000 years ago and its unfinished termination. Quat. Sci. Rev. 114, 52–60.
Shulmeister, J., Fink, D., Hyatt, O.M., Thackray, G.D., Rother, H., 2010. Cosmogenic ^{10}Be and ^{26}Al exposure ages of moraines in the Rakaia Valley, New Zealand and the nature of the last termination in New Zealand glacial systems. Earth Planet Sci. Lett. 297, 558–566.
Shulmeister, J., Fink, D., Winkler, S., Thackray, G.D., Borsellino, R., Hemmingsen, M., Rittenour, T.M., 2019a. Evidence for slow late-glacial ice retreat in the upper Rangitata Valley, South Island, New Zealand. Quat. Sci. Rev. 185, 102–112.
Shulmeister, J., Thackray, G.D., Rittenour, T.M., Fink, D., 2019b. The timing and nature of the last glacial cycle in New Zealand. Quat. Sci. Rev. 206, 1–20.
Sikes, E.L., Guilderson, T.P., 2016. Southwest Pacific Ocean surface reservoir ages

since the last glaciation: circulation insights from multiple-core studies. Paleoceanography 31, 298–310.
Sikes, E.L., Nodder, S.D., Volkman, J.K., 2005. Alkenone temperature records and biomarker flux at the subtropical front on the Chatham Rise, SW Pacific Ocean. Deep-Sea Res. I 52, 721–748.
Singh, G., Geissler, E.A., 1985. Lake Cainozoic history of vegetation, fire, lake levels and climate, at Lake George, New South Wales, Australia. Phil. Trans. Roy. Soc. Lond. B 311, 379–447.
Sniderman, J.M.K., Hellstrom, J., Woodhead, J.D., Drysdale, R.N., Bajo, P., Archer, M., Hatcher, L., 2019. Vegetation and climate change in southwestern Australia during the last glacial maximum. Geophys. Res. Lett. 46 https://doi.org/10.1029/2018GL080832.
Sprigg, R.C., 1979. Stranded and submerged sea-beach systems of Southeast South Australia and the aeolian desert cycle. Sediment. Geol. 22, 53–96.
Sprigg, R.C., 1982. Some stratigraphic consequences of fluctuating Quaternary sea levels and related wind regimes in southern and central Australia. In: Wasson, R.J. (Ed.), Quaternary Dust Mantles of Chiba, New Zealand and Australia. Australian National University, Canberra, pp. 211–240.
Strand, P.D., Schaefer, J.M., Putnam, A.E., Denton, G.H., Barrell, D.J.A., Koffman, T.N.B., Schwartz, R., 2019. Millennial-scale pulsebeat of glaciation in the southern Alps of New Zealand. Quat. Sci. Rev. 220, 165–177.
Stuiver, M., Reimer, P.J., 1993. Extended ^{14}C data base and revised CALIB 3.0 14C age calibration program. Radiocarbon 35, 215–230.
Stuut, J.-B.W., De Deckker, P., Saavedra-Pellitero, M., Bassinot, F., Drury, A.-J., Walczak, M.H., Kana Nagashima, K., Murayama, M., 2019. A 5.3-million-year history of monsoonal precipitation in northwestern Australia. Geophys. Res. Lett. 46 https://doi.org/10.1029/2019GL083035.
Stuut, J.-B., Temmesfeld, F., De Deckker, P., 2014. A 550 kyr record of aeolian activity near North 2014. A 550 ka record of aeolian activity near North West Cape, Australia: inferences from grain-size distributions and bulk chemistry of SE Indian Ocean deep-sea sediments. Quat. Sci. Rev. 83, 83–94.
Tjallingii, R., Röhl, U., Kölling, M., Bickert, T., 2007. Influence of the water content on X-ray fluorescence core-scanning measurements in soft marine sediments. G-cubed 8, Q02004. https://doi.org/10.1029/2006GC001393.
Toggweiler, J.R., Russell, J.L., Carson, S.R., 2006. Mid latitude westerlies, atmospheric CO_2, and climate change during the ice ages. Paleoceanography 21, PA2005. https://doi.org/10.1029/2005PA001154.
Turney, C.S.M., Haberle, S., Fink, D., Kershaw, A.P., Barbetti, M., Barrows, T.T., Black, M., Cohen, J.T., Correge, T., Hesse, P.P., Hua, Q., Johnston, R., Morgan, V., Moss, P., Nanson, G., van Ommen, T., Rule, S., Williams, N.J., Zhao, J.-X., D'Costa, D., Feng, Y.-X., Gagan, M., Mooney, S., Xia, Q., 2006. Integration of ice core, marine and terrestrial records for the Australian Last Glacial Maximum and Termination: a contribution from the OZ INTIMATE group. J. Quat. Sci. 21, 751–761.
van der Kaars, S., De Deckker, P., 2002. A Late Quaternary pollen record from deep-sea core Fr10/95-GC17 offshore Cape Range Peninsula, northwestern Western Australia. Rev. Palaeobot. Palynol. 120, 17–39.
van der Kaars, S., De Deckker, P., 2003. Pollen distribution in marine surface sediments offshore Western Australia. Rev. Palaeobot. Palynol. 124, 113–129.
van der Kaars, S., Miller, G.H., Turney, C.S.M., Cook, E.J., Nürnberg, D., Schönfeld, J., Kershaw, A.P., Lehman, S.T., 2018. Humans rather than climate the primary cause of Pleistocene megafaunal extinction in Australia. Nat. Commun. 8, 14142. https://doi.org/10.1038/ncomms14142.
Veth, P., 2017. Breaking through the radiocarbon barrier: Madjedbebe and the new chronology for Aboriginal occupation of Australia. Aust. Archaeol. 83, 165–167.
Veth, P., Ward, I., Ditchfield, K., 2017. Reconceptualising Last Glacial Maximum discontinuities: a case study from the maritime deserts of north-western Australia. J. Anthropol. Archaeol. 46, 82–91.
Ward, I., Veth, P., McDonald, J., McNear, S., 2018. Recognition and value of submerged prehistoric landscape resources in Australia. Ocean Coast Manag. 160, 167–174.
Weltje, G.J., Tjallingii, R., 2008. Calibration of XRF core scanners for quantitative geochemical logging of sediment cores: theory and application. Earth Planet Sci. Lett. 274, 423–438.
Wijffels, S., Beggs, H., Griffin, C., Middleton, J.F., Cahill, M., King, E., Feng, M., Benthuysen, J.A., Steinberg, G.R., Sutton, P., 2018. A fine spatial-scale sea surface temperature atlas of the Australian regional seas (SSTAARS): seasonal variability and trends around Australasia and New Zealand revisited. J. Mar. Syst. 187, 156–196.
Williams, M.A.J., Prescott, J.R., Chappell, J., Adamson, D., Cock, B., Walker, K, Gell, P., 2001. The enigma of a late Pleistocene wetland in the Flinders Ranges, South Australia. Quat. Int. 83-85, 129–144.
Williams, A.N., Ulm, S., Smith, M., Reid, J., 2014. AustArch: a database of ^{14}C and non-^{14}C ages from archaeological sites in Australia - composition, compilation and review (data paper). Internet Archaeol. 36 https://doi.org/10.11141/ia.36.6 [The dataset has been deposited with the Archaeology Data Service doi: 10.5284/1027216].
Williams, M.A.J., Ambrose, S.H., van der Kaars, S., Ruehlemann, C., Chattopadhyaya, U., Pal, J., Chauhan, P.R., 2009a. Environmental impact of the 73 ka Toba super-eruption in south Asia. Palaeogeogr. Palaeoclimatol. Palaeoecol. 295–314.
Williams, M.A.J., Cook, E., van der Kaars, S., Barrows, T., Shulmeister, J., 2009b. Glacial and deglacial patterns in Australia and surrounding regions from 35 000 to 10 000 years ago reconstructed from terrestrial and near-shore proxy data. Quat. Sci. Rev. 28, 2398–2419.
Williams, P.W., 1996. A 230 ka record of glacial and interglacial events from Aurora Cave, Fiordland, New Zealand. N. Z. J. Geol. Geophys. 39, 225–241.
Williams, P.W., Neil, H., Zhao, J.-X., 2010. Age frequency distribution and revised stable isotope curves for New Zealand speleothems: palaeoclimatic implications. Int. J. Speleol. 39, 99–112.
Wood, R., 2017. Comments on the chronology of Madjedbebe. Aust. Archaeol. 83, 172–174.
Yokoyama, Y., et al., 2018. Rapid glaciation and a two-step sea level plunge into the Last Glacial Maximum. Nature org/10.1038/s41586-018-0335-4.